

## Article

# Crystal Nanoarchitectonics and Characterization of the Octahedral Iron(III)–Nitrate Complexes with Isomer Dimethylurea Ligands

Kende Attila Béres <sup>1,2</sup> , Zoltán Homonnay <sup>3</sup>, Laura Bereczki <sup>1,4</sup>, Zsolt Dürvanger <sup>5,6</sup> ,  
Vladimir M. Petruševski <sup>7</sup> , Attila Farkas <sup>8</sup>  and László Kótai <sup>1,9,\*</sup> 

- <sup>1</sup> Institute of Materials and Environmental Chemistry, Research Centre for Natural Sciences, H-1117 Budapest, Hungary; beres.kende.attila@ttk.hu (K.A.B.); nagyne.bereczki.laura@ttk.mta.hu (L.B.)  
<sup>2</sup> György Hevesy PhD School of Chemistry, ELTE Eötvös Loránd University, H-1117 Budapest, Hungary  
<sup>3</sup> Institute of Chemistry, ELTE Eötvös Loránd University, H-1117 Budapest, Hungary; homonnay.zoltan@ttk.elte.hu  
<sup>4</sup> Centre for Structural Science, Research Centre for Natural Sciences, H-1117 Budapest, Hungary  
<sup>5</sup> ELKH-ELTE Protein Modelling Research Group, H-1117 Budapest, Hungary; zsolt.durvanger@ttk.elte.hu  
<sup>6</sup> Structural Chemistry and Biology Laboratory, Institute of Chemistry, ELTE Eötvös Loránd University, H-1117 Budapest, Hungary  
<sup>7</sup> Faculty of Natural Sciences and Mathematics, Ss. Cyril and Methodius University, MK-1000 Skopje, North Macedonia; vladop@pmf.ukim.mk  
<sup>8</sup> Department of Organic Chemistry and Technology, Faculty of Chemical Technology and Biotechnology, Budapest University of Technology and Economics, H-1111 Budapest, Hungary; farkas.attila@vbk.bme.hu  
<sup>9</sup> Deuton-X Ltd., H-2030 Érd, Hungary  
\* Correspondence: kotai.laszlo@ttk.hu

**Abstract:** Three octahedral iron(III) nitrate complexes with dimethylated urea ligand isomers, [hexakis(*N,N'*-dimethylurea-O)iron(III)] nitrate (compound **1**), trans-[diaquatetakis(*N,N*-dimethylurea-O)iron(III)] nitrate (compound **2**), and [hexakis(*N,N*-dimethylurea-O)iron(III)] nitrate trihydrate (compound **3**) were prepared and characterized with single crystal X-ray diffraction, IR, Raman and UV–Vis methods. In compounds **1** and **3**, six dimethylurea ligands coordinate to the central Fe<sup>III</sup> ion via the oxygen in octahedral geometry and the ligands are arranged in a propeller-like manner, dividing the complex cations into two sides. In compound **1**, the dimethylurea propellers screw in the opposite direction on the two sides of the complex and in compound **3**, they are arranged with the same handedness on the two sides. The complexes have helical chirality. The two sides of the complex cations differ not only in the rotation direction of the ligands but also in the hydrogen bond formation. On one side of the complex cation, the ligands form intermolecular hydrogen bonds only with the crystal waters, meanwhile on the other side of the complex, the ligands form hydrogen bonds only with the nitrate ions. In compound **2**, [Fe(*N,N*-dimethylurea)<sub>4</sub>(H<sub>2</sub>O)<sub>2</sub>]<sup>3+</sup> cations form layers that are separated by interconnected NO<sub>3</sub><sup>−</sup> ions forming a hydrogen bonding system and connecting the complex cations *A*-s and *B*-s. The three crystallographically different nitrate ions each form four hydrogen bonds in a way that they have one bidentate O atom and two monodentate O atoms; however, the anions differ in their hydrogen bonding. The spectroscopic characteristics of compound **2** were determined by IR measurements on the deuterated compound **2** as well.

**Keywords:** crystal structure; dimethylurea isomers; complexes; IR spectroscopy; UV spectroscopy



**Citation:** Béres, K.A.; Homonnay, Z.; Bereczki, L.; Dürvanger, Z.; Petruševski, V.M.; Farkas, A.; Kótai, L. Crystal Nanoarchitectonics and Characterization of the Octahedral Iron(III)–Nitrate Complexes with Isomer Dimethylurea Ligands. *Crystals* **2023**, *13*, 1019. <https://doi.org/10.3390/cryst13071019>

Academic Editor: Marian Valko

Received: 16 June 2023

Revised: 21 June 2023

Accepted: 24 June 2023

Published: 27 June 2023



**Copyright:** © 2023 by the authors. Licensee MDPI, Basel, Switzerland. This article is an open access article distributed under the terms and conditions of the Creative Commons Attribution (CC BY) license (<https://creativecommons.org/licenses/by/4.0/>).

## 1. Introduction

The quasi-intramolecular solid phase redox reactions of complexes having oxidizing anions and reducing ligands are extensively studied in inorganic chemistry [1–19]. The heat-induced solid phase processes of complexes [ML<sub>*n*</sub>](XO<sub>4</sub>)<sub>*m*</sub> (M = Fe, Cu, Zn, Co; L = urea, NH<sub>3</sub> or pyridine, and *n* = 2–6; X = Mn, Mo, Cl, S, and *m* = 0.5–3 [1–15] ensure a

convenient way to prepare simple or mixed nanosized transition metal oxides that proved to be excellent catalysts in various industrial processes such as the Fischer–Tropsch synthesis [16–19]. The key point of triggering these solid phase redox reactions is the existence of hydrogen bonds between the potential redox active components of the complexes [1–4,6–9]. In order to explore new precursor complexes with advantageous thermal decomposition features and with useful decomposition product properties, some complexes with methyl substituted urea ligands, including iron(III) nitrate complexes with dimethylated urea isomers (*N,N* (1,1-dimethylurea)) and (*N,N'* (1,3-dimethylurea)) have been prepared. Due to the key parameter, the existence of hydrogen bonds between *N,N*- and *N,N'*-dimethylurea ligands and nitrate ions have enormous importance from the point of view of further investigations. In this paper, we present our results about the preparation and crystal structure of three new complexes, [hexakis(*N,N'*-dimethylurea-O)iron(III)] nitrate (compound 1), trans-[diaquatetrakis(*N,N*-dimethylurea-O)iron(III)] nitrate (compound 2), and [hexakis(*N,N*-dimethylurea-O)iron(III)] nitrate trihydrate (compound 3). In order to characterize the influence of the hydrogen bonds in compounds 1–3, detailed spectroscopic (IR, Raman, and UV–Vis) studies were also performed.

Numerous crystallographically characterized unsubstituted urea complexes of iron(III) salts are known (ESI Table S1), whereas only two complexes of iron(III) perchlorate with methyl or ethyl substituted urea ligands have been structurally characterized until now [1,2,20–25]. Neither diaquo-complexes of asymmetric dimethylurea with metals nor its hexacoordinated complexes with trivalent metals has been structurally characterized. There are four structurally characterized isomorphous monoclinic complexes with divalent Mn, Co, Ni, and Zn cations known (ESI Table S1). There are only five examples of crystallographically characterized symmetric dimethylurea complexes. Among them, one is an iron(III) complex with perchlorate anion (monoclinic), the other four complexes that are formed with divalent metals are triclinic.

The urea and its derivatives can coordinate to the central metal atoms via the oxygen of the carbonyl group or via one of the nitrogens of the amino groups (in a few cases, it coordinates as a bidentate ligand) [26,27]. The complexes of trivalent cations ( $\text{Mn}^{\text{III}}$ ,  $\text{Fe}^{\text{III}}$ ) [1,2,28–33] are mostly O-coordinated compounds [1,2,21–25,28–32]. The methyl substitution of the urea ligand is expected to be of great influence on the hydrogen bond systems with the respective anion of the iron(III) salts due to the electron density shift inside the urea molecule and due to steric factors as well. Thus, because of structural changes, the ability of the urea–iron(III) complexes to show heat-induced quasi-intermolecular redox reactions will surely be altered. Some octahedral iron(III) complexes containing urea with various anions ( $\text{Cl}^-$ ,  $\text{Br}^-$ ,  $\text{NO}_3^-$ ,  $\text{ClO}_4^-$ ,  $\text{MnO}_4^-$ , and  $\text{S}_2\text{O}_8^{2-}$ ) have been studied with several spectroscopic methods [1,2,22–33], and the most extensively studied iron(III)–urea complex is clearly the  $[\text{Fe}(\text{urea})_6](\text{NO}_3)_3$  [25,26]. Thus, to clarify the effect of methyl substitution in the ligand on the properties of N–H $\cdots$ O interactions, we selected the iron(III) complexes of dimethyl substituted urea isomers (*N,N*- and *N,N'*-) with nitrate counter ions.

## 2. Materials and Methods

Chemical grade iron(III) nitrate nonahydrate, *N,N*-dimethylurea, *N,N'*-dimethylurea, and urea and the analytical reagents or solvents were supplied by Deuton-X Ltd., Érd, Hungary. The syntheses of compounds 1–3 were based on the previously described methods [1,2,22–25,31–33].

### 2.1. [Hexakis(*N,N'*-dimethylurea-O)iron(III)] Nitrate (Compound 1)

Compound 1 was prepared in the following way: iron(III) nitrate nonahydrate (8.08 g, 0.02 mol) and *N,N'*-dimethylurea (10.6 g, 0.12 mol) were dissolved in 12 mL of distilled water. The light orange solution was slowly evaporated at 25 °C. After a week, orange colored block-like crystals were formed that were filtered off and then washed first in water, then in abs. ethanol and finally in diethyl ether. The yield was 88%.

## 2.2. [Diaquatetrakis(*N,N*-dimethylurea-*O*)iron(III)] Nitrate (Compound 2) and [Hexakis(*N,N*-dimethylurea-*O*)iron(III)] Nitrate Trihydrate (Compound 3)

Compounds **2** and **3** were prepared in the following way: iron(III) nitrate nonahydrate (8.08 g, 0.02 mol) and *N,N*-dimethylurea (10.6 g, 0.12 mol) were dissolved in 13.5 mL of distilled water and the deep orange solution was left to evaporate at room temperature. Two kinds of orange crystals were formed, the prism-like ones were identified as [diaquatetrakis(*N,N*-dimethylurea-*O*)iron(III)] nitrate (compound **2**), and the needle-like crystals were proven to be the expected [hexakis(*N,N*-dimethylurea-*O*)iron(III)] nitrate trihydrate (compound **3**). The further slow evaporation of the mother liquor resulted in only compound **2** after four days. The yield was 93%. Compound **2** was the main product, whereas compound **3** was a byproduct formed in a small amount.

The same reaction conditions were used for the  $\text{Fe}(\text{NO}_3)_3 \cdot 9\text{H}_2\text{O}$  to *N,N*-dimethylurea molar ratios 1:4 and 1:8. At ratio 1:4, the final product was only compound **2**; however, when the Fe to *N,N*-dimethylurea ratio in the reaction mixture was 1:8, first the excess (2 mol) *N,N*-dimethylurea crystallized and after that only compound **2** formed. Based on these observations, the formation of compound **2** is favorable against compound **3**.

## 2.3. Powder X-ray Diffractometry

Powder X-ray tests were performed with a Philips PW-1050 Bragg–Brentano parafocusing goniometer equipped with a copper cathode (40 kV, 35 mA, secondary beam graphite monochromator, proportional counter). Scans were recorded in step mode, and the diffraction patterns were evaluated with a full profile fitting technique [34,35].

## 2.4. Single Crystal X-ray Diffraction

The single crystal X-ray diffraction measurements on compound **1** and **3** were done at 100 and 105 K, respectively. Intensity data were collected on a Rigaku XtaLAB Synergy R, HyPix diffractometer (rotating anode X-ray tube, PhotonJet R X-ray source, mirror monochromator; Cu- $K_\alpha$  radiation,  $\lambda = 1.54184 \text{ \AA}$ ) [1]. The cell parameters were determined by the least-squares method, and analytical absorption correction was applied to the data. The structure was solved with the intrinsic phasing method as implemented in SHELXT [36]. Refinement was carried out using SHELXL [37] and Olex2 [38] with full matrix least squares method on  $F^2$ . Hydrogen atoms were included in the structure factor calculation, but they were not refined. The isotropic displacement parameters of the hydrogen atoms were approximated from the  $U(\text{eq})$  value of the atom they were bonded to. Olex2 [38] and Mercury [39] were used for molecular graphics and analyzing crystal packing.

The single crystal X-ray diffraction measurement on compound **2** was done at 113 K. Intensity data were collected on a Rigaku R-Axis Rapid diffractometer (graphite monochromator; Mo- $K_\alpha$  radiation,  $\lambda = 0.71073 \text{ \AA}$ ). Hydrogen atomic positions were calculated from assumed geometries. Hydrogen atoms were included in structure factor calculations but they were not refined. The isotropic displacement parameters of the hydrogen atoms were approximated from the  $U(\text{eq})$  value of the atom they were bonded to.

Crystal data and details of the structures' refinement are listed in Table 1 and ESI Tables S2–S10. The CCSD numbers are 2,267,946 (compound **1**), 2,267,944 (compound **2**), and 2,267,945 (compound **3**).

**Table 1.** Crystal data and structure refinement of compounds **1**, **2** and **3**.

Label	Compound 1	Compound 2	Compound 3
Compound	$[\text{Fe}(\text{N,N}'\text{-DMU})_6](\text{NO}_3)_3$	$[\text{Fe}(\text{N,N}'\text{-DMU})_4(\text{H}_2\text{O})_2](\text{NO}_3)_3$	$[\text{Fe}(\text{N,N}'\text{-DMU})_6](\text{NO}_3)_3 \cdot 3\text{H}_2\text{O}$
Empirical formula	$\text{C}_{18}\text{H}_{48}\text{FeN}_{15}\text{O}_{15}$	$\text{C}_{12}\text{H}_{36}\text{FeN}_{11}\text{O}_{15}$	$\text{C}_{18}\text{H}_{54}\text{FeN}_{15}\text{O}_{18}$
Formula weight	770.56	630.37	824.61
Temperature	100.00(10)	113(2)	105(2) K
Radiation and wavelength	Cu- $K_\alpha$ , $\lambda = 1.54184 \text{ \AA}$	Mo- $K_\alpha$ , $\lambda = 0.71073 \text{ \AA}$	Cu- $K_\alpha$ , $\lambda = 1.54184 \text{ \AA}$
Crystal system	Trigonal	Triclinic	Trigonal

Table 1. Cont.

Label	Compound 1	Compound 2	Compound 3
Space group	R-3	P-1	R-3
Unit cell dimensions	$a = 12.1232(2)\text{Å}$ $b = 12.1232(2)\text{Å}$ $c = 22.5665(4)\text{Å}$ $\alpha = 90^\circ$ $\beta = 90^\circ$ $\gamma = 120^\circ$	$a = 9.8655(6)\text{Å}$ $b = 10.5568(7)\text{Å}$ $c = 15.5569(10)\text{Å}$ $\alpha = 77.658(5)^\circ$ $\beta = 76.538(5)^\circ$ $\gamma = 62.239(4)^\circ$	$a = 22.0051(3)\text{Å}$ $b = 22.0051(3)\text{Å}$ $c = 13.9132(2)\text{Å}$ $\alpha = 90^\circ$ $\beta = 90^\circ$ $\gamma = 120^\circ$
Volume	2872.30(11) $\text{Å}^3$	1383.86(16) $\text{Å}^3$	5834.51(18) $\text{Å}^3$
Z	3	2	6
Density (calculated)	1.337 Mg/m <sup>3</sup>	1.513 Mg/m <sup>3</sup>	1.408 Mg/m <sup>3</sup>
Absorption coefficient, $\mu$	3.844 mm <sup>-1</sup>	0.629 mm <sup>-1</sup>	3.887 mm <sup>-1</sup>
$F(000)$	1221	662	2622
Crystal color	orange	orange	orange
Crystal description	block	prism	rod
Crystal size	0.39 × 0.37 × 0.29 mm	0.37 × 0.33 × 0.32 mm <sup>3</sup>	0.197 × 0.066 × 0.049 mm <sup>3</sup>
Absorption correction	Gaussian	numerical	Gaussian
Max. and min. transmission	0.2790.328	0.9070.962	1.0000.569
$\Theta$ -range for data collection	4.645 ≤ $\Theta$ ≤ 75.409°	5.116 ≤ $\Theta$ ≤ 25.349°	3.934 ≤ $\Theta$ ≤ 75.583°
Index ranges	−15 ≤ $h$ ≤ 15; −15 ≤ $k$ ≤ 14; −28 ≤ $l$ ≤ 28	−11 ≤ $h$ ≤ 11; −12 ≤ $k$ ≤ 12; −18 ≤ $l$ ≤ 18	−27 ≤ $h$ ≤ 27; −27 ≤ $k$ ≤ 27; −17 ≤ $l$ ≤ 17
Reflections collected	13,522	22,946	27,109
Completeness to 2 $\Theta$	1.000	0.990	100.0%
Independent reflections	1324 [R(int) = 0.0395]	5030 [R(int) = 0.0547]	2672 [R(int) = 0.0466]
Refinement method	full-matrix least-squares on $F^2$	full-matrix least-squares on $F^2$	full-matrix least-squares on $F^2$
Data/restraints/parameters	1321/20/96	5030/1/363	2672/0/164
Goodness-of-fit on $F^2$	1.113	1.114	1.088
Final R indices [ $I > 2\sigma(I)$ ]	R1 = 0.0577, wR2 = 0.1672	R1 = 0.0504, wR2 = 0.1032	R1 = 0.0417, wR2 = 0.1233
R indices (all data)	R1 = 0.0577, wR2 = 0.1673	R1 = 0.0660, wR2 = 0.1089	R1 = 0.0427, wR2 = 0.1242
Largest diff. peak and hole	0.978; −0.803 e.Å <sup>-3</sup>	0.445; −0.326 e.Å <sup>-3</sup>	0.522; −0.376 e.Å <sup>-3</sup>

### 2.5. Infrared Spectroscopy

The far-IR and mid-IR spectra of compound **1**, **2**, and **2-D**<sub>12</sub> were recorded using the attenuated total reflection technique (ATR). The details of the instrumentation (BioRad-Digilab FTS-30-FIR and Bruker Alpha IR spectrometers) were given in [2]. The far-IR and FT-IR measurements were carried out between 400 and 40 cm<sup>-1</sup> and 4000 and 400 cm<sup>-1</sup>, respectively.

### 2.6. Raman Spectroscopy

The Raman spectroscopic measurement was done between room temperature and −180 °C on a Horiba Jobin-Yvon LabRAM microspectrometer. Two external diode laser sources were applied (785 nm diode and 532 nm frequency-doubled Nd:YAG) (~80 mW and 40 mW, respectively) and an Olympus BX-40 (Evident Co., Tokyo, Japan) optical microscope was used. A Linkam THMS600 (Empire Optics Co., New York, NY, USA), temperature-controlled microscope stage was used in the low-temperature measurements. The laser beam was focused by an objective of 20×. Due to the heat-sensitivity of compound **1**, a D0.3 intensity filter, in the case of compound **2**, a D0.6 (−180 °C) and a D1 (25 °C) were used for excitation with Nd:YAG laser to decrease the laser power to 50%, 25%, and 10%, respectively. For light dispersion, the confocal hole of 1000 μm and a monochromator with 950 (785 nm) and 1800 (532 nm) groove mm<sup>-1</sup> grating were used. The resolution was 4 cm<sup>-1</sup>, and the exposure times were 20 s, exceptionally 120 s at the highest power filtering.

### 2.7. UV–Vis Spectroscopy

The UV–Vis spectra were recorded in diffuse reflectance mode, the details of the instrumentation were given in [40] (Jasco V-670 UV–Vis instrument, an NV-470 integrating sphere, BaSO<sub>4</sub> as standard).

## 3. Results and Discussion

The prism and needle-like orange crystals of compounds **2** and **3**, respectively, were prepared from aq. iron(III) nitrate nonahydrate and six equivalents of *N,N*-dimethylurea solutions with slow evaporation at room temperature. Upon further slow evaporation of

the mother liquor, only compound **2** was obtained. For the same reaction conditions at  $\text{Fe}(\text{NO}_3)_3 \cdot 9\text{H}_2\text{O}$  to  $N,N$ -dimethylurea molar ratio of 1:4 and 1:8, the final product was only compound **2** and a mixture of free  $N,N$ -dimethylurea ligand and compound **2**, respectively.

### 3.1. Single Crystal Structure of Compounds 1–3

Single-crystal X-ray diffraction measurements were performed on the orange, block-like crystals of [hexakis( $N,N'$ -dimethylurea- $\text{O}$ )iron(III)] nitrate (compound **1**) and on the orange rod-like crystals (needles) of [hexakis( $N,N$ -dimethylurea- $\text{O}$ )iron(III)] nitrate trihydrate (compound **3**). Measurement conditions and cell parameters are listed in Table 1. Both compound **1** and compound **3** crystallized from aqueous solution by slow evaporation of the solvent in the trigonal crystal system and  $R\bar{3}$  space group. Orange prism-like crystals of [diaquatetrakis( $N,N$ -dimethylurea- $\text{O}$ )iron(III)] nitrate (compound **2**) were grown from the same solution together with compound **3** and measured by single-crystal X-ray diffraction. Compound **2** crystallized in the triclinic crystal system and  $P\bar{1}$  space group. The cell parameters for compounds 1–3 are given in Table 1. The calculated and the experimental powder X-ray diffraction patterns agree well for compounds **1** and **2** (ESI Figures S1 and S2, the differences in the intensities of peaks in the experimental and calculated PXRDs may be attributed to orientation effects) and there was no sign of structural change between  $-140$  and  $20$  °C on DSC spectra (ESI Figures S3 and S4).

In compounds **1** and **3**, six dimethylurea ligands coordinate to the central  $\text{Fe}^{\text{III}}$  ion via the oxygen in octahedral geometry (Figure 1a,b). Dimethylurea ligands are arranged in a propeller-like manner, dividing the complex cations into two sides, as characteristic of hexaurea transition metal complexes. In compound **1**, the dimethylurea propellers screw in the opposite direction on the two sides of the complex and in compound **3**, they are arranged with the same handedness on the two sides. In compound **2**, two of the  $N,N$ -dimethylurea ligands are exchanged for water in the coordination sphere of iron (Figure 1c). The accidental replacement of the urea ligands with water within the coordination sphere of the central metal ion can also be observed at  $\text{Mn}^{\text{II}}$ ,  $\text{Co}^{\text{II}}$ ,  $\text{Ni}^{\text{II}}$ , and  $\text{Zn}^{\text{II}}$  analogs [41–44].

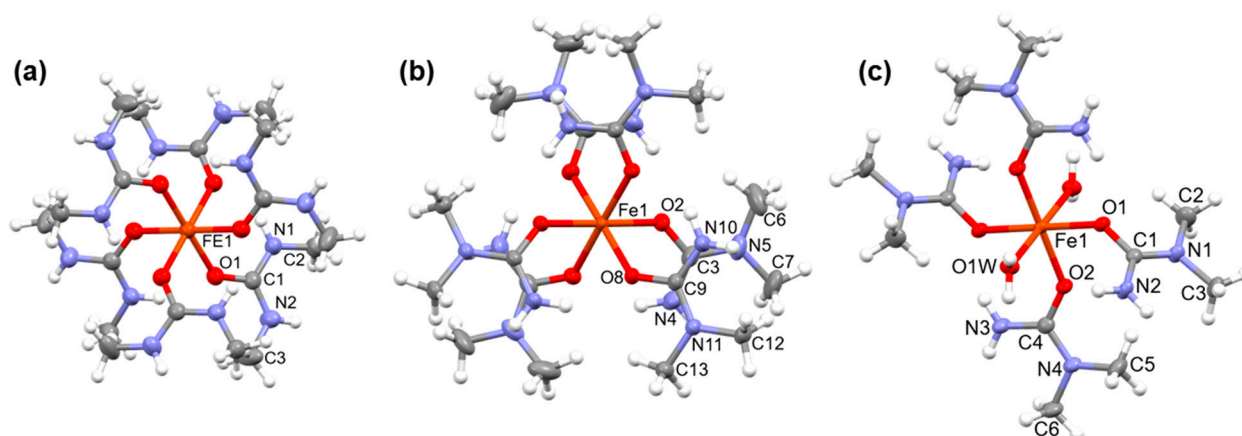


**Figure 1.** Comparison of the structures of the complex cations in (a) compound **1** [ $\text{Fe}(\text{N},\text{N}'\text{-dimethylurea})_6]^{3+}$ , (b) compound **3** [ $\text{Fe}(\text{N},\text{N}\text{-dimethylurea})_6]^{3+}$ , and (c) compound **2** [ $\text{Fe}(\text{N},\text{N}\text{-dimethylurea})_4(\text{H}_2\text{O})_2]^{3+}$ ] (Ellipsoid representation, thermal ellipsoids are drawn at the 50% probability level.).

The different positions of the methyl groups on the urea ligands and the partial substitution of the urea ligands with water in the coordination sphere of iron result in basically different packing arrangements of the complexes (Figure 2). In compound **1**, the complex cations are sandwiched between two nitrate anions and the resulting “ionic sandwiches” are arranged in columns running parallel to the crystallographic  $c$  direction. However, these sandwiching nitrates have hydrogen bond interactions only with the complex cations in the neighboring columns and not with the cations that they straddle. Their interaction

with the straddling nitrate ions is rather an ionic interaction with the positively charged coordination sphere of the  $\text{Fe}^{3+}$  ion. A large number of intramolecular hydrogen bridges are formed between the dimethylurea ligands of the  $[\text{hexakis}(\text{dimethylurea-O})\text{iron(III)}]^{3+}$  cations that consume the hydrogen bond donor and acceptor abilities of the inside of the coordination sphere of iron and no hydrogen bonds can be formed under and above the cations. Therefore, the cations interact with the nitrate ions only with their external functional groups. Between the nitrate- $[\text{Fe}(\text{N,N}'\text{-dimethylurea})_6]^{3+}$ -nitrate sandwiches, two strongly disordered nitrate anions fill the space each with half occupancy. In compound **3**, the complex cations form columns that are separated by distinct columns of the nitrate anions. The neighboring complex cations within one column do not have any hydrogen bond interactions with each other only radially with the nitrate ions. In compound **2**, layers of the complex cations are separated by nitrate layers. The  $[\text{diaquatetrakis}(\text{N,N}'\text{-dimethylurea-O})\text{iron(III)}]^{3+}$  cations are able to form hydrogen bonds even axially, through their water ligands.

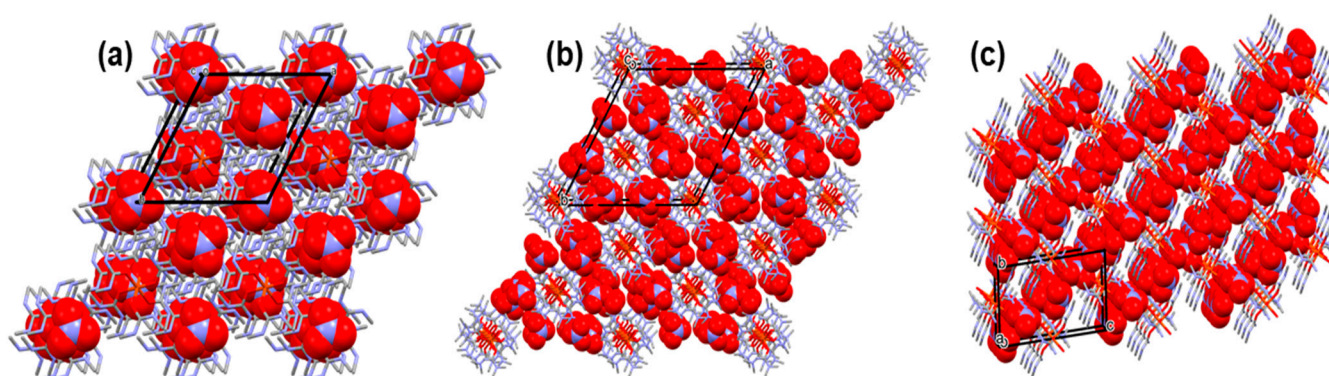


**Figure 2.** Packing arrangements of (a) compound **1**, (b) compound **3**, and (c) compound **2**. (Complex cations are drawn with stick representation and nitrate anions with space fill representation).

In compound **1**, all coordinative Fe-O bond lengths are equal, 2.004(1) Å; however, the O-Fe-O angles show a slight distortion from the octahedral geometry, since they are 92.13(6)° and 87.87(6)°. The bond lengths and angles are listed in ESI Table S2. This distortion is more remarkable than that in the complex cation of the perchlorate salt ( $[\text{Fe}(\text{N,N}'\text{-dimethylurea})_6](\text{ClO}_4)_3$ ), where the O-Fe-O bond angles vary between 88.19 and 91.81° (ESI Table S3). The distortion of the complex cation of compound **1** is caused by the internal hydrogen bond system (Figure 3). The Fe-O distances in the perchlorate salt are between 1.989 and 2.023 Å, whereas the Fe...Fe interatomic distances are 10.038 and 10.278 Å in the nitrate and perchlorate salt, respectively. The other bond distances and angles were found to be very close to those found for other dimethylurea complexes (ESI Table 1).

The H1 amide hydrogens facing the interior part of the complex cation get close to the coordinated O1 atoms of the neighboring *N,N'*-dimethylurea ligands and in this arrangement, an intramolecular hydrogen bond is formed between them. The result of this hydrogen bonding is that the ligands *A* are “pulled down” and the ligands *B* are “pulled up” which causes the distortion of the complex (Figure 3a).

Beside the internal hydrogen bonding, the H2 amine hydrogens of *N,N'*-DMU ligands form intermolecular hydrogen bonds with the  $\text{NO}_3^-$  anions (2.05 Å). Each  $\text{NO}_3^-$  ion forms three identical hydrogen bonds with three different complex cations (Figure 3b,c) and the nitrate anions are symmetric, i.e., the N-O bond lengths are uniformly 1.252(2) Å and the O-N-O angles are 120.00°. The C-O bond length increases from 1.242 to 1.283(2) upon coordination as compared to the uncoordinated *N,N'*-dimethylurea [1]. Furthermore, the N1-C-N2 bond lengths become asymmetric in the complex, one of them becomes longer and the other becomes shorter (from 1.329 to 1.335(3) and 1.324(3), respectively) [1]. For these changes, the coordination and the different hydrogen bond strengths are responsible.

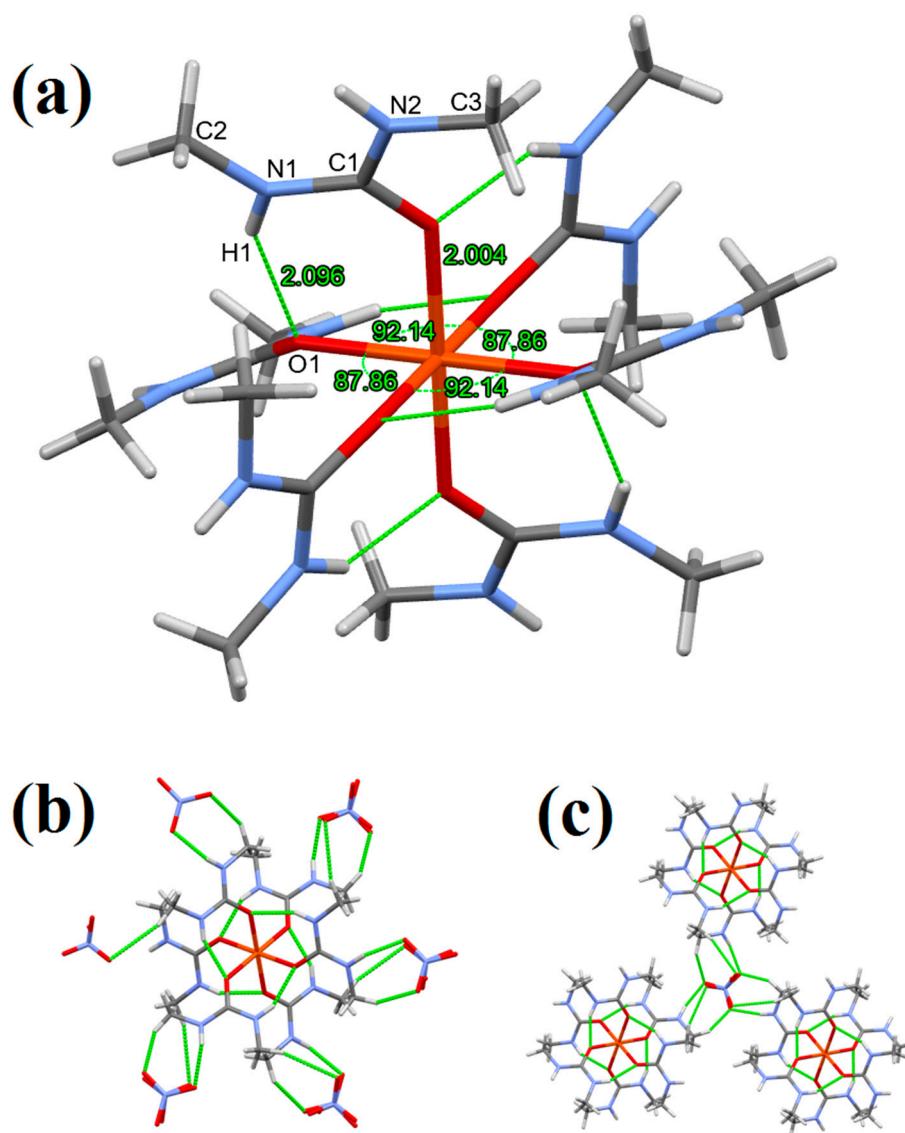


**Figure 3.** (a) Coordination geometry, intramolecular hydrogen bonding, (b,c) hydrogen bonding in compound 1 (stick representation, hydrogen bonds are drawn by green dashed lines).

In compound **3**, the six coordinated *N,N*-dimethylurea ligands are placed around the  $\text{Fe}^{3+}$  ion in an octahedral geometry and are arranged in a propeller-like manner, dividing the complex into two sides and the rotation direction of the ligands are different at the two sides of the complex. This way, the complex has a helical chirality. This arrangement is similar to the  $[\text{Fe}(\text{urea})_6]^{3+}$  cation [1,2]; however, it differs from that in compound **1** (Figure 1b). The two sides of the complex cations differ not only in the rotation direction of the ligands but also in the hydrogen bond formation. On one side of the complex cation, the ligands form intermolecular hydrogen bonds only with the crystal waters, meanwhile on the other side of the complex, the ligands form hydrogen bonds only with the  $\text{NO}_3^-$  ions (Figure 4). These differences result in different Fe-O bond lengths on the two sides of the complex cation of compound **3**, three 2.009(1) Å and three 2.017(1) Å bond lengths were measured, the shorter one belongs to the side where hydrogen bonds are formed only with the water molecules (Figure 4). Due to these effects, there is a slight distortion in the octahedral geometry of the complex cation of compound **3** (ESI Tables S6 and S7). The O-Fe-O angles prove to have distorted octahedral geometry too, as they vary between 88.70° and 91.19° (ESI Figure S5).

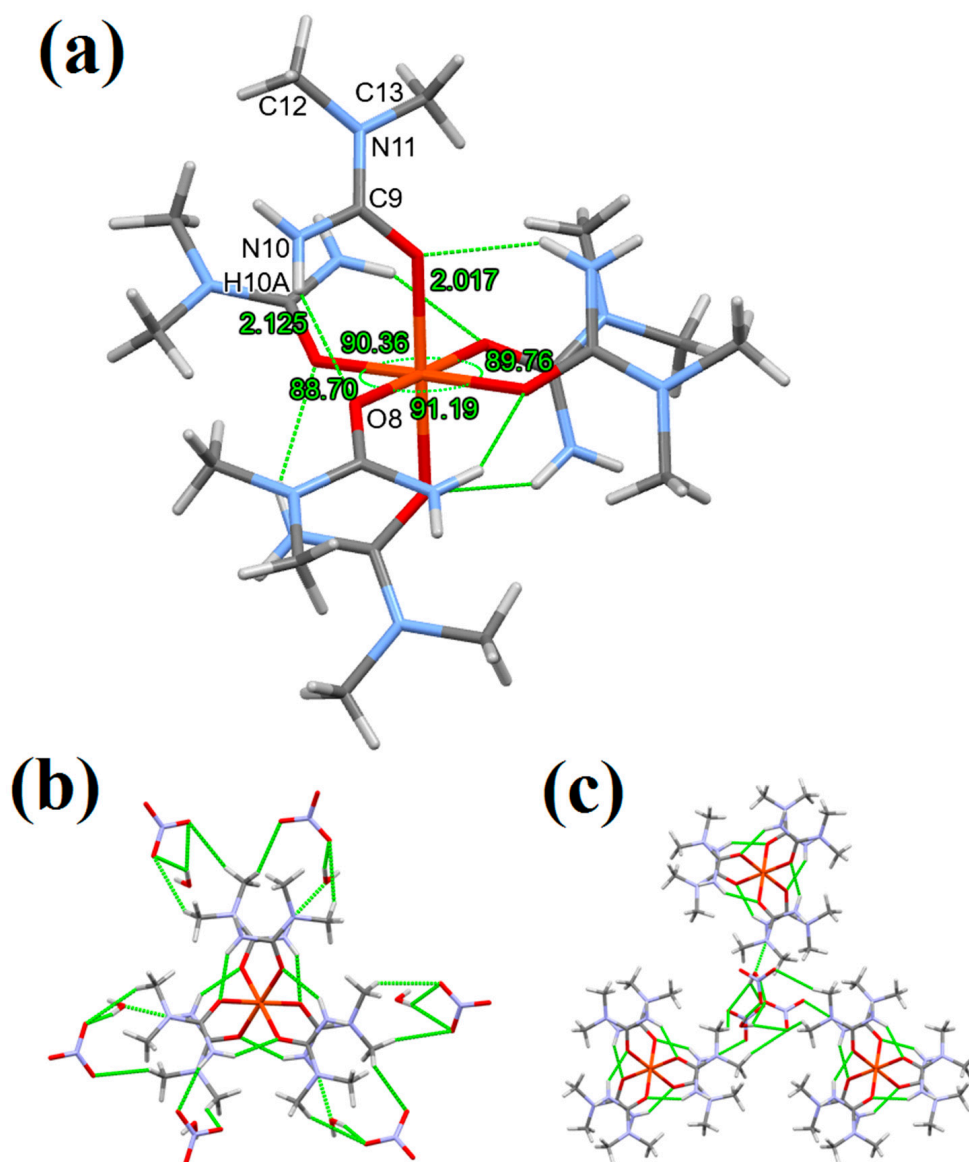


**Figure 4.** (a) Coordination geometry, intramolecular hydrogen bonding, (b,c) hydrogen bonding in compound **3** (stick representation, hydrogen bonds are drawn by green dashed lines).

One of the H atoms of the  $\text{-NH}_2$  groups (the one facing inside) on each ligand forms an intramolecular hydrogen bond with the coordinated O atom of the neighboring ligand, all together six internal hydrogen bonds just like in the  $[\text{M}(\text{N,N-dimethylurea})_6]^{2+}$  ( $\text{M} = \text{Mn}^{\text{II}}$ ,  $\text{Co}^{\text{II}}$ ,  $\text{Ni}^{\text{II}}$  and  $\text{Zn}^{\text{II}}$  complex cations [41–44]). The other H atoms of the  $\text{-NH}_2$  groups (facing outside) form intermolecular hydrogen bonds with the nitrate anions or water molecules (Figure 4). The methyl groups on the N5 and N11 atoms of complex cation of compound **3** are facing outside of the center of the complex cation due to the steric hindrance (Figure 1c) and these groups do not form any hydrogen bonds (Figure 4). Similarly to the compound **1** structure, in compound **3**, the  $[\text{Fe}(\text{N,N-dimethylurea})_6]^{3+}$  cations form columns along the  $c$  unit cell axis (Figure 3b). The columns are filled with interconnected  $\text{NO}_3^-$  anions and water molecules forming a hydrogen bonding system. Each of the O atoms of the  $\text{NO}_3^-$  ions form hydrogen bonds: one O atom with the complex cation, one with hydrogen of one water molecule, and one with the H atoms of two different water molecules (bidentate), resulting in structurally distorted anions with three non-equivalent N–O bond lengths: 1.243(2) Å (connected to the complex cation), 1.243(2) Å (connected to one water molecule), and 1.251(2) Å (connected to two water molecules) (ESI Figure S6). The O atom of each

water molecule forms hydrogen bond with the complex cations. Both H atoms of the water molecules form H bonds as well: one with one O atom and one with two of the  $\text{NO}_3^-$  ions (ESI Figure S6). This hydrogen bond system is similar to the  $\text{Mn}^{\text{II}}$ ,  $\text{Co}^{\text{II}}$ ,  $\text{Ni}^{\text{II}}$ , and  $\text{Zn}^{\text{II}}$ -*N,N*-dimethylurea analogue complexes [41–44].

In compound **2**, in contrast to compound **3**, only four *N,N*-dimethylurea (equatorial) and two water (axial) molecules coordinate to the central  $\text{Fe}^{3+}$  atom forming an octahedral coordination geometry (Figure 1c). The crystallization of compound **2** seems energetically more favorable, since from the reaction solution (described in Section 2.2), a large amount of compound **2** formed (at the whole area of the solution) and a small amount of compound **3**. Our assumption was confirmed by changing the condition of the synthesis: when the reaction mixture contained a 1:4 molar ratio of Fe to *N,N*-dimethylurea, only crystals of compound **2** formed. Two different complex cations can be found in the unit cell of compound **2** (*A* and *B*) with a slight distortion from the octahedral symmetry with different Fe–O bond lengths. The Fe–O bond lengths which belong to the coordinated water molecules are different: 2.026(2) (complex cation *A*) and 2.033(2) Å (complex cation *B*). In both complex cations, the H atoms of the coordinated water molecules differ: the H1(WB) and H2(WB) form monodentate-, while H1(WA) and H2(WA) form a bidentate hydrogen bond (Figure 5). In complex cation *A*, the H1(WB) hydrogen binds to an O atom of a nitrate anion, whereas in complex cation *B*, the H2(WB) binds to the O atom of a nitrate anion, which has a hydrogen bond with the *N,N*-dimethylurea ligand (the neighbor of the coordinated water molecule) (Figure 5) (the Fe–O bond length is 2.026(2) Å). In the complex cations *A* and *B* of compound **2**, the *N,N*-dimethylurea ligands can be divided into two groups: *N,N*-dimethylurea ligands *I* have shorter Fe–O bond lengths (1.960 and 1.970 Å) *N,N*-dimethylurea ligands *II* having longer bonds (2.002 and 2.009 Å). The shorter Fe–O bond lengths (1.960 and 2.002 Å) belong to the complex cation *A*. The hydrogen bonding system is also responsible for the differences. The  $-\text{NH}_2$  groups of *N,N*-dimethylurea ligands *I* form one intramolecular (with the O atom of neighboring *N,N*-dimethylurea ligand *II*) and one intermolecular (with a bidentate O atom of a  $\text{NO}_3^-$  ion) hydrogen bond, while the  $-\text{NH}_2$  groups of the *N,N*-dimethylurea ligands *II* form two intermolecular hydrogen bonds (with two different  $\text{NO}_3^-$  ion) (Figure 5). In complex cation *A* and *B*, ligands *I* differ in the intermolecular hydrogen bond lengths (2.081 and 2.090 Å, respectively) and in the (N-)H-O(-N)-H(-O) angle of the bidentate nitrate anion (176.2 and 108.6, respectively) (Figure 5). In complex cation *A* and *B*, ligands *II* differ in the angles enclosed by the two nitrate anions and the  $-\text{NH}_2$  group of the ligand (( $\text{O}_2\text{N}$ )-O-N-O(- $\text{NO}_2$ )), being 96.4 and 120.6°, respectively (Figure 5).

Unlike the structures of compounds **1** and **3**, in compound **2**  $[\text{Fe}(\text{N,N}\text{-dimethylurea})_4(\text{H}_2\text{O})_2]^{3+}$  cations form layers (Figure 2c) that are separated by interconnected  $\text{NO}_3^-$  ions forming a hydrogen bonding system and connecting the complex cations *A*-s and *B*-s. Three crystallographically different nitrate anions can be found in each cationic column, and all three kinds are slightly distorted (the N–O bond lengths and O–N–O angles are listed in ESI Table S11). The three nitrate ions form four hydrogen bonds in a way that they have one bidentate O atom and two monodentate O atoms (ESI Figure S7); however, the anions differ in their hydrogen bondings.  $\text{NO}_3^-$  *A* and *B* connect three different complex cations via hydrogen bonding, but the bonding angles of their bidentate bonded O atoms differ (176.2° and 108.6°, respectively). Meanwhile,  $\text{NO}_3^-$  *C* is connected to two different parts of two different complex cations: the bidentate O atom is connected to the H of a coordinated water molecule and a H of the amino group of the coordinated *N,N*-dimethylurea, while one monodentate O atom is coordinated to the H of the a water molecule, and another monodentate O atom is coordinated to the H of the amino group of the *N,N*-dimethylurea. The hydrogen bonding system in compound **2** resembles more the  $\text{Mn}^{\text{II}}$ ,  $\text{Co}^{\text{II}}$ ,  $\text{Ni}^{\text{II}}$ , and  $\text{Zn}^{\text{II}}$  *N,N*-dimethylurea complexes than compounds **1** and **3** since there are more crystallographically different  $\text{NO}_3^-$  and all of them have bidentately connected O atoms to different complex cations [41–44]. In both complex cations of compound **2**, only two intramolecular hydrogen bonds can be found, which is much less than the 6 intramolecular hydrogen

bonds in both compounds **1** and **3**. This is due to the asymmetric methylation of urea, the two coordinated water molecule, and the propeller-like structure of the complex cations. In this way, only two amino groups face the center of the complex cations and are close enough to the neighboring O atom of the coordinated *N,N*-dimethylurea ligands. The other two coordinated *N,N*-dimethylurea ligands and the two coordinated water molecules form only intermolecular hydrogen bonds with two different nitrate anions. A similar effect was recognized in the case of  $\text{Mn}^{\text{II}}$ ,  $\text{Co}^{\text{II}}$ ,  $\text{Ni}^{\text{II}}$ , and  $\text{Zn}^{\text{II}}$  complexes, where with the decrease of the *N,N*-dimethylurea ligands the number of internal hydrogen bonds decrease as well (and become zero in the case of  $[\text{M}(\text{N,N-dimethylurea})_2(\text{H}_2\text{O})_4]^{2+}$  ( $\text{M} = \text{Mn}^{\text{II}}$ ,  $\text{Co}^{\text{II}}$ ,  $\text{Ni}^{\text{II}}$ , and  $\text{Zn}^{\text{II}}$ ) [41–44].

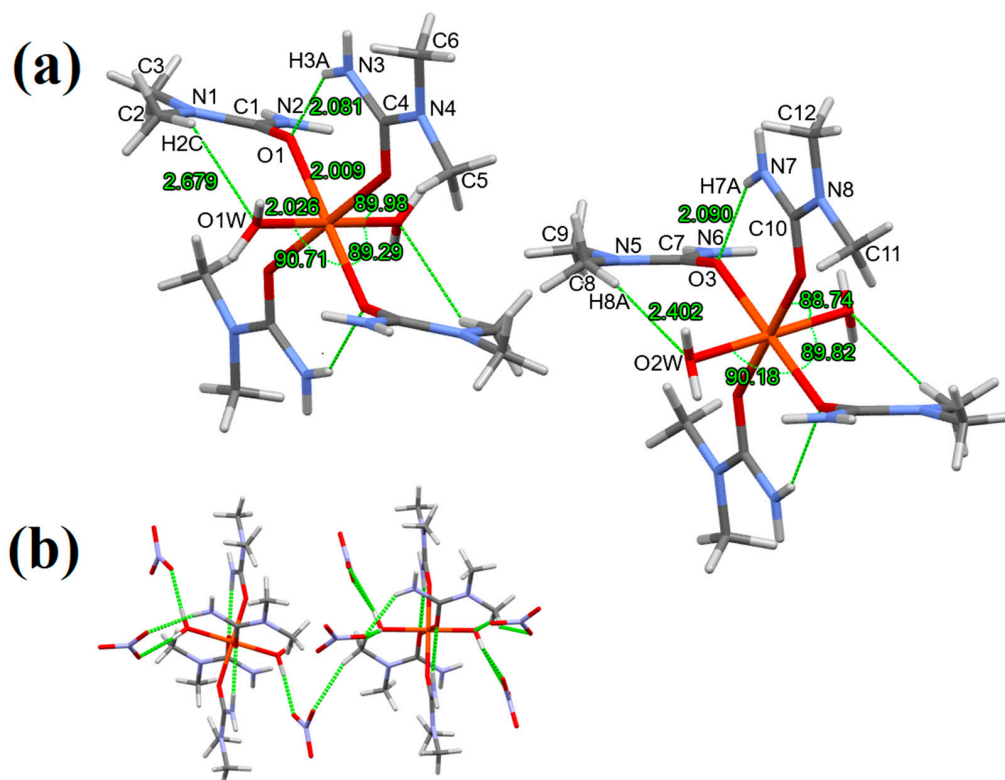


**Figure 5.** (a) Coordination geometry, intramolecular hydrogen bonding, (b) hydrogen bonding in compound **1** (stick representation, hydrogen bonds are drawn by green dashed lines).

In compound **1**, two Fe-Fe distances were found between the neighboring  $[\text{Fe}(\text{N,N}'\text{-dimethylurea})_6]^{3+}$ : 10.275 Å and 12.123 Å, the shortest is similar to the analogue perchlorate complex (10.038 Å) (ESI Figure S8) [23]. The Fe-Fe distances in compound **3** are much shorter than in compounds **1** and **2**, and are similar to the Me-Me distances in the  $\text{Co}^{\text{II}}$ ,  $\text{Ni}^{\text{II}}$ , and  $\text{Zn}^{\text{II}}$  analogues, the shortest distances are 6.633 and 7.280 Å (ESI Figure S9). The shortest Fe-Fe distance in [diaquatetrakis(*N,N*-dimethylurea)iron(III)] nitrate is longer than that in compound **3** and shorter than that in compound **1**, so it is closer to the  $\text{Co}^{\text{II}}$ ,  $\text{Ni}^{\text{II}}$ , and  $\text{Zn}^{\text{II}}$  *N,N*-dimethylurea complexes. Its value is 9.388 Å (ESI Figure S10) [41–44].

### 3.2. Vibrational Spectrum of Compound **1**

The room temperature IR spectra of compound **1** ([hexakis(*N,N'*-dimethylurea)iron(III)] nitrate) has partly been evaluated by Masłowska et al. [45], but there are no available data about the far-IR and Raman studies of this compound. The results of the IR (room temperature) and Raman (room temperature and liq.  $\text{N}_2$  temperature) measurements on compound **1** and the assignments of the vibrational modes are given in ESI Figures S11 and S12 and ESI Table S12. The results of the correlation analysis for the nitrate ions are given in Figure 6.

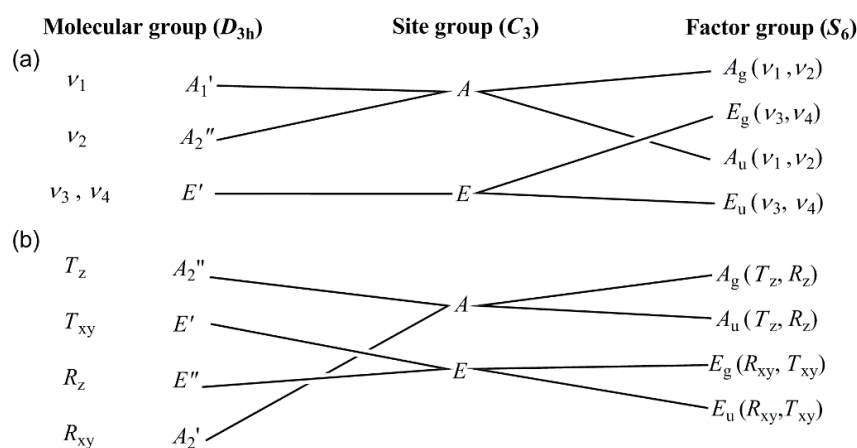


**Figure 6.** (a) Internal and (b) external  $\text{NO}_3^-$  modes in compound **1**.

The N-H stretching mode region contains four IR and five Raman bands, whereas Masłowska found only one wide IR band in this region [45]. The appearance of these bands might be attributed to the presence of the two crystallographically different cations (A and B—Figure 2a, Section 3.1), the non-equivalence of ligands in the trans- and cis-octahedral positions, and the distorted nature of the octahedral cations, or because the  $N,N'$ -dimethylurea ligand has a considerable double-bond character, the relative positions of two imides and the carbonyl groups. The (cis,trans)-configuration of the free  $N,N'$ -dimethylurea is less favorable [46] and less symmetric than the trans, trans, and (cis,cis)-configurations, but the coordination to iron(III) and the hydrogen bonds fix the ligands in this configuration causing splitting and shifting the  $\nu_s(\text{N-H})$  and  $\nu_{as}(\text{N-H})$  bands as compared to the  $\nu_s(\text{N-H})$  and  $\nu_{as}(\text{N-H})$  modes of the free ligand.

The room temperature and low-temperature Raman spectra ( $-80$  and  $-180$  °C) show that the lowering of the temperature resulted in the splitting of the Raman bands (ESI Figures S12 and S13). Similar reasons explain the increase in the number of bands belonging to symmetric and antisymmetric C-H modes of the methyl groups in the IR and Raman spectra, respectively (Figure 7 and ESI Tables S12 and S13a).

The band observed at  $3111\text{ cm}^{-1}$  in the IR spectrum of compound **1** might belong to the strongest N-H bond facing outside of the complex cation of compound **1**, bonded to a nitrate anion (the smallest length and angle difference between the cations A and B were observed for this hydrogen bonding environment (discussed in Section 3.1). Making this assumption, we can expect that these N-H bonds of ligands A and B energetically do not differ enough to result in splitting or making a shoulder/widening of the band belonging to these fragments. The band positions of  $\nu_s(\text{C-H})$  and  $\nu_{as}(\text{C-H})$  modes in the IR spectrum of compound **1** slightly differ from the results given by Mido [46] due to the different configurations of the free (trans, trans) and the complexed (cis,trans) ligand in compound **1**. A temperature dependence could be observed in the Raman spectra similar to that found for  $\nu(\text{N-H})$  bands (Figure 7a, ESI Table S12). The amide I, II, and III bands belong to the mixed modes of  $\nu(\text{C=O})$ ,  $\nu(\text{C-N})$ , and  $\delta(\text{NH})$  and are located at  $1625\text{ cm}^{-1}$ ,  $1596\text{ cm}^{-1}$ , and  $1266\text{ cm}^{-1}$  in the IR spectrum of the free ligands, respectively. The greatest contribution of  $\nu(\text{C=O})$  is expected in the amide I band and a lesser contribution of  $\nu(\text{C=O})$  is expected in the amide II band. Accordingly, due to the C=O coordination “pile-up” and “spill-over” effects, the amide I and II bands observed in the IR spectrum of compound **1** were shifted to  $1621\text{ cm}^{-1}$  and  $1595\text{ cm}^{-1}$ , respectively. The higher shift of the amide I band than the amide II band confirms the higher contribution of  $\nu(\text{C=O})$  mode in the amide I than in the amide II band. The splitting of amide I and II bands may be attributed to the influence of the (cis,trans)-NH, or axial/equatorial ligand arrangements. The main components in the amide II band are the  $\nu(\text{C-N})$  and the  $\delta(\text{NH})$  modes (ESI Table S12), whereas the main component of the amide III band is the  $\delta(\text{NH})$ , and additional components are  $\nu(\text{CN})$  and  $\nu(\text{C'-N})$ . A strong band at  $1336\text{ cm}^{-1}$ , and two bands at  $1280$  and  $1255\text{ cm}^{-1}$  appeared.

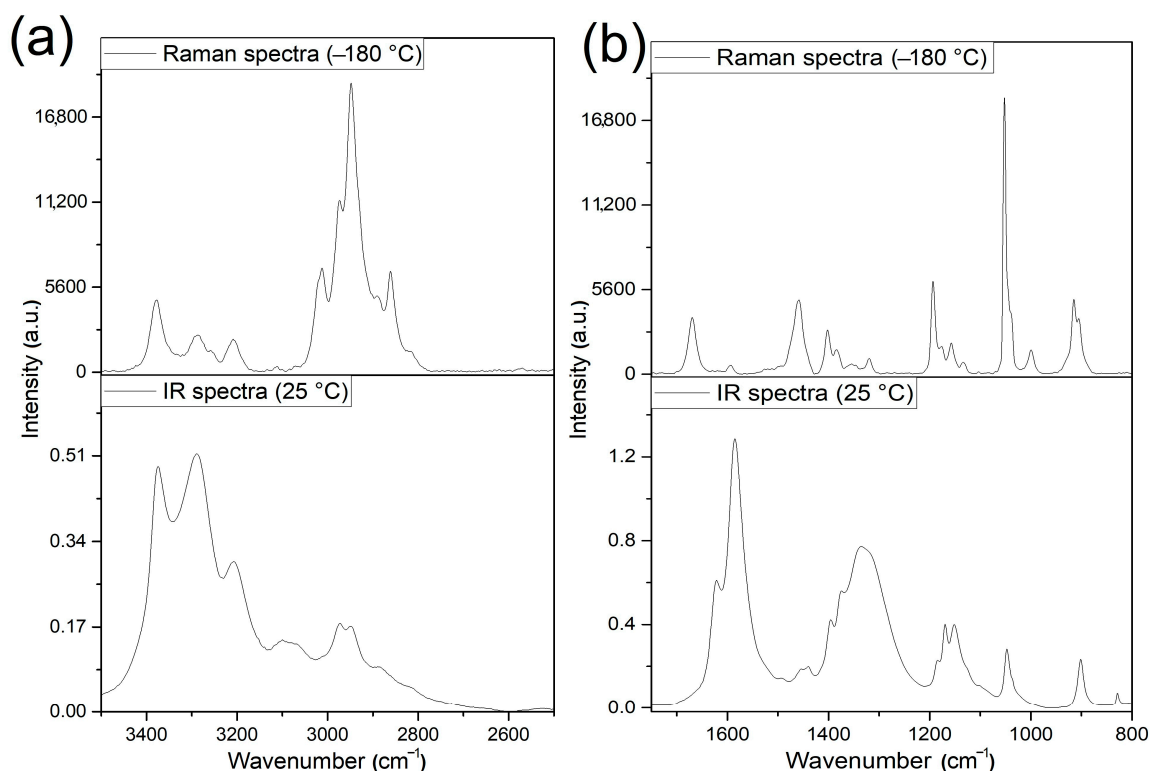


**Figure 7.** The IR (room temperature) and Raman ( $-180\text{ }^{\circ}\text{C}$ ) spectra of compound **1** in (a) the N-H and C-H bond stretching mode and (b) in the amide bands ranges.

The band at  $1336\text{ cm}^{-1}$  may be attributed to the presence of the (cis,trans)-conformer, because the solution phase IR spectrum of the free ligand contains a band at this position (due to rotation of the dissolved species) [46], which cannot be seen in the solid (frozen) sample. The Raman spectra recorded at liq.  $\text{N}_2$  temperature showed an unresolved wide band around  $1669\text{ cm}^{-1}$  (amide I), whereas the amide II and III bands are weak due to low Raman intensity of CN and N-H modes (Figure 7b, ESI Figure S13c,d and ESI Table S12). The symmetric deformation mode of methyl groups and a combined band of  $\nu(\text{C}'\text{N})$  and rocking mode of methyl groups are expected to be in the band position range of the antisymmetric and symmetric stretching modes of the nitrate ion. Therefore, a correlation analysis has been done to determine the number and splitting of the expected modes of the nitrate anion in compound **1** (Figure 6). The intensity of the antisymmetric and symmetric N-O modes of the nitrate ion is higher and lower in the IR and then the Raman spectra, respectively. The isolated  $D_{3h}$  nitrate ion has three IR active ( $\nu_2$ ,  $\nu_3$ , and  $\nu_4$ ) and three Raman active ( $\nu_1$ ,  $\nu_3$ , and  $\nu_4$ ) modes. The symmetry decrease causes all four normal modes to become IR and Raman active in the spectra of compound **1**.

There are two formula units in the primitive cell, the site group is  $C_3$ , and the factor group is  $S_6$ . We can expect two ( $\nu_1$  and  $\nu_2$ ) singlet IR ( $A_u$ ) and Raman ( $A_g$ ) and two ( $\nu_3$  and  $\nu_4$ ) doubly degenerate IR ( $E_u$ ) and Raman ( $E_g$ ) bands. The  $A_g$  and  $A_u$  rotational and translational ( $R_z$ ,  $T_z$ ) modes are singlets, whereas the  $E_g$  and  $E_u$  rotational and translational modes ( $R_{xy}$ ,  $T_{xy}$ ) are doubly degenerate. Considering the singlet nature of  $\nu_1$  (N-O) band, among the four experimentally found bands with weak/medium intensity at 1099, 1064, 1047, and  $1037\text{ cm}^{-1}$ , in the IR spectrum, three belong to the  $\nu(\text{C}'\text{-N})$  and  $\rho(\text{CH}_3)$  mixed bands of ligands, and only one may belong to the nitrate ion (Figure 7b). The Raman spectrum recorded at low temperature unambiguously shows a very strong narrow singlet at  $1052\text{ cm}^{-1}$ , which is much more intense than the other bands, thus it is assigned as  $\nu_1(\text{NO}_3)$  in the Raman spectrum. One among the bands located at 1064 or  $1047\text{ cm}^{-1}$  in the IR spectrum might belong to the  $\nu_1(\text{NO}_3)$  mode and the other to a mixed  $N,N'$ -dimethylurea ligand band. Since no N-H-containing species contributes to the mixed

ligand bands, we cannot distinguish these bands by deuteration. However, the nitrate ion  $\nu_1(\text{NO}_3)$  mode in compound **2** was assigned at  $1044\text{ cm}^{-1}$  (see below); thus, the band at  $1047\text{ cm}^{-1}$  probably belongs to the nitrate ion  $\nu_1(\text{NO}_3)$  mode in the IR spectrum of compound **1**. The  $\nu_2$  band of the nitrate ion was found at  $829$  and  $762\text{ cm}^{-1}$  as a doublet in the IR spectrum of compound **1**, the Raman intensity of this deformation mode is low (ESI Figure S13e,f). The antisymmetric stretching mode of nitrate ion appears as a doublet both in the IR and Raman spectra, at  $1396/1374\text{ cm}^{-1}$  and  $1402/1384\text{ cm}^{-1}$ , respectively (ESI Figure S13c,d). The intensities of these bands are much lower in the Raman than in the IR spectrum. The well-separated bands around  $1300$  (IR) and  $1330\text{ cm}^{-1}$  (Raman) are close to the expected range of the  $\nu_3(\text{NO}_3)$  mode belonging to the mixed  $\delta(\text{NH})$ ,  $\nu(\text{CN})$ ,  $\nu(\text{C}'\text{N})$ , and  $\nu(\text{C}=\text{O})$  modes (ESI Table S12). The  $\nu_4(\text{N}-\text{O})$  mode (deformation) is located at  $724/707$  and  $729/716\text{ cm}^{-1}$  in the IR and Raman spectra, respectively (Figure 7 and ESI Figure S13g,h). The bands belonging to Fe-O coordination of the cations types *A* and *B* were found at  $389\text{ cm}^{-1}$  in the IR as a wide band with shoulders and at  $420$  and  $383\text{ cm}^{-1}$  in the low-temperature Raman spectra (ESI Figure S12 and ESI Table S12). The lattice modes appear in the far-IR spectra at  $303$ ,  $248$ ,  $157$ , and  $129\text{ cm}^{-1}$  (ESI Figure S11a).

### 3.3. Vibrational Spectrum of Compound 2

Compound **2** ([diaquatetrakis(*N,N*-dimethylurea)iron(III)] nitrate) has not been prepared previously, therefore there are no available spectroscopic data about it. The equatorial positions are filled only with *N,N*-dimethylurea ligands, whereas the axial position is filled only with water ligands. One would expect the resonance structures to contribute less to the spectral characteristics (due to the lack of  $\text{NH}-\text{C}(=\text{O})-\text{NH}$  linkage) than in the complexes with *N,N'*-dimethylurea [46]. The IR and Raman spectroscopic data (the latter measured at both room temperature and liq.  $\text{N}_2$  temperature) together with the IR spectrum of the perdeuterated derivative (**2-D<sub>12</sub>**, the ligands are  $\text{Me}_2\text{NCOND}_2$  and  $\text{D}_2\text{O}$ ) are given in Figures 8 and 9, ESI Table S13 and ESI Figures S14–S16.

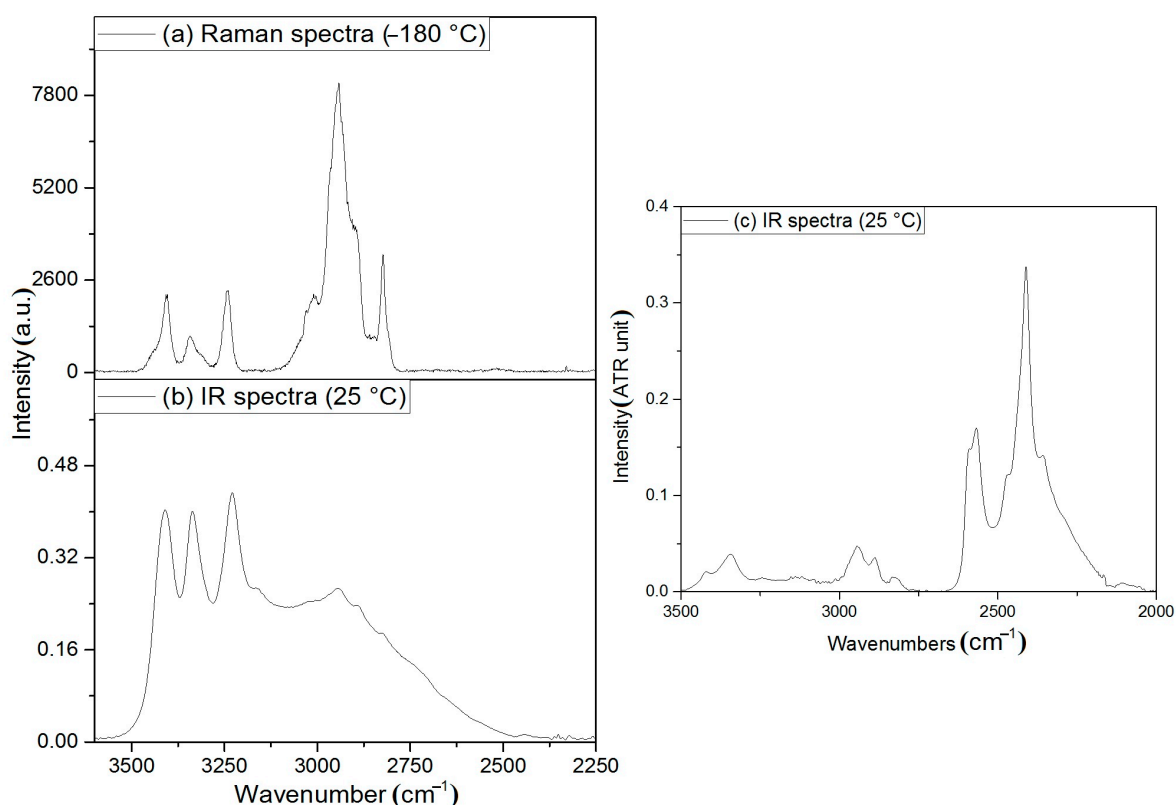


**Figure 8.** (a): Raman ( $-180\text{ }^\circ\text{C}$ ), (b): IR (room temperature) spectra of compound **2**, and (c): IR (room temperature) spectra of compound **2-D<sub>12</sub>** in the N-H and C-H bond stretching mode range.

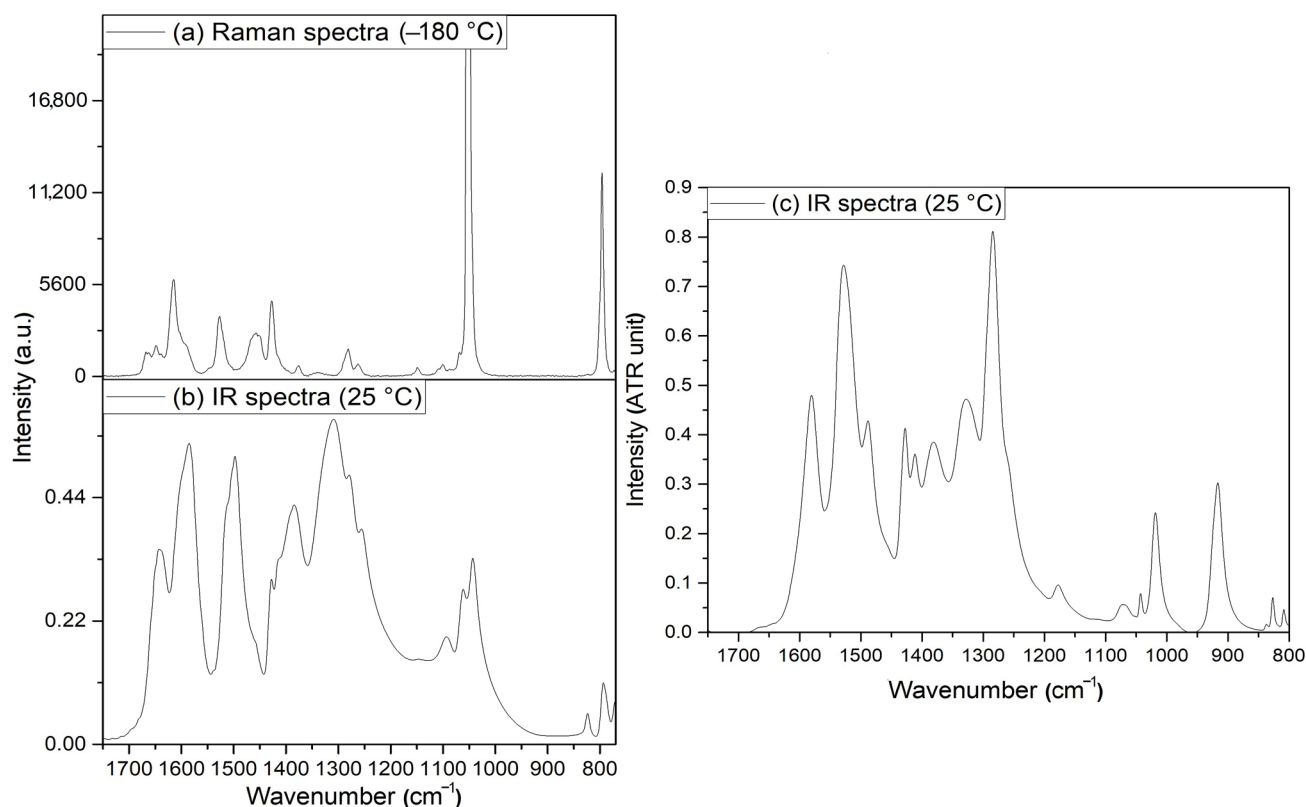


**Figure 9.** (a) Raman ( $-180\text{ }^{\circ}\text{C}$ ) spectra and (b) IR (room temperature) of compound **2** and (c) IR (room temperature) spectra of compound **2-D<sub>12</sub>** in the amide bands range.

Since the structure consists of relatively strong hydrogen bonds by  $\text{NH}_2$  groups and  $\text{H}_2\text{O}$  ligands (Figure 8), the symmetric/antisymmetric OH and NH bands appear in the IR spectrum of compound **2** at  $3410$  and  $3336/3229/3159\text{sh cm}^{-1}$ . The band at the highest wavenumber belongs to the coordinated water, whereas the other two bands and the shoulder may belong to the symmetric and antisymmetric modes of  $\text{NH}_2$  group. The deuteration experiments resulted in four bands in the IR spectrum of compound **2-D<sub>12</sub>** (Figures 8c and 9c and ESI Figure S14). The  $\nu(\text{OH})/\nu(\text{OD})$  ratio is  $1.33$ , whereas the  $\nu(\text{NH})/\nu(\text{ND})$  ratio is varied between  $1.37$  and  $1.45$  due to the difference in the strength of hydrogen bonds between the amino group hydrogens and electron donating groups. The band at  $1641\text{ cm}^{-1}$  is located close to the amide I band of the free ligand ( $1642\text{ cm}^{-1}$ ). This band completely disappears on deuteration, while a somewhat broad band appears in the IR spectrum of compound **2-D<sub>12</sub>** between  $1190$  and  $1160\text{ cm}^{-1}$ . Thus, this band and the shoulder can be assigned to the  $\delta(\text{OH})$  scissoring modes of the coordinated and crystal water. The amide I band of the coordinated ligand is located at  $1585\text{ cm}^{-1}$  in the IR spectrum of compound **2** and contains  $\nu(\text{C}=\text{O})$ ,  $\nu(\text{C}-\text{N})$ , and  $\delta(\text{NH})$  contributions. The  $\delta(\text{NH})/\delta(\text{ND})$  ratio in the free ligand was found to be  $1.37$  [46], and accordingly, the  $\delta(\text{ND})$  mode coincides with the experimentally found wide band system between  $1190$  and  $1160\text{ cm}^{-1}$  in the IR spectrum of compound **2-D<sub>12</sub>** (Figure 9c and ESI Figure S14 and ESI Table S13). The amide II IR band is found at  $1514/1497\text{ cm}^{-1}$ , and the component of  $1497\text{ cm}^{-1}$  disappeared on deuteration, whereas the component at  $1520\text{ cm}^{-1}$  remained. Thus, the components at  $1497$  and  $1514\text{ cm}^{-1}$  in the IR spectrum of compound **2** belong to  $\delta(\text{NH}_2)$  and C-N mode contributions, respectively, and the  $\delta(\text{ND}_2)$  component appears at  $1071\text{ cm}^{-1}$  in the IR spectrum of the deuterated compound ( $\delta(\text{NH})/\delta(\text{ND}) = 1.40$ ). The  $\delta_r$  mode of  $\text{NH}_2$  group in the IR spectrum of compound **2** appeared at  $1094\text{ cm}^{-1}$ , and using the  $\delta_r(\text{NH})/\delta_r(\text{ND})$  value given for the free ligand ( $1.27$ ) by [46], the new intense band at  $912\text{ cm}^{-1}$  in the IR spectrum of compound **2-D<sub>12</sub>** can be assigned to  $\delta_r(\text{ND}_2)$ . The  $\delta_r(\text{Me})$  and  $\nu_s(\text{CN})$  combined band located at  $1062\text{ cm}^{-1}$  shifts on deuteration only slightly, and

splits into two bands at 1044 and 1023  $\text{cm}^{-1}$ , representing separated  $\delta_r(\text{Me})$  and  $\nu_s(\text{CN})$ , respectively. The  $\nu_s(\text{CN})$  band is expected to be more sensitive to deuteration following the logic of mechanically coupled oscillators.

The  $\nu_{\text{as}}(\text{N-O})$  nitrate bands are expected to be in the range of  $\delta_s(\text{CH}_3)$  modes ( $\sim 1400 \text{ cm}^{-1}$ ) of the *N,N*-dimethylurea ligand [46] (ESI Table S13). The correlation analysis of the nitrate ion is given in Figure 10.

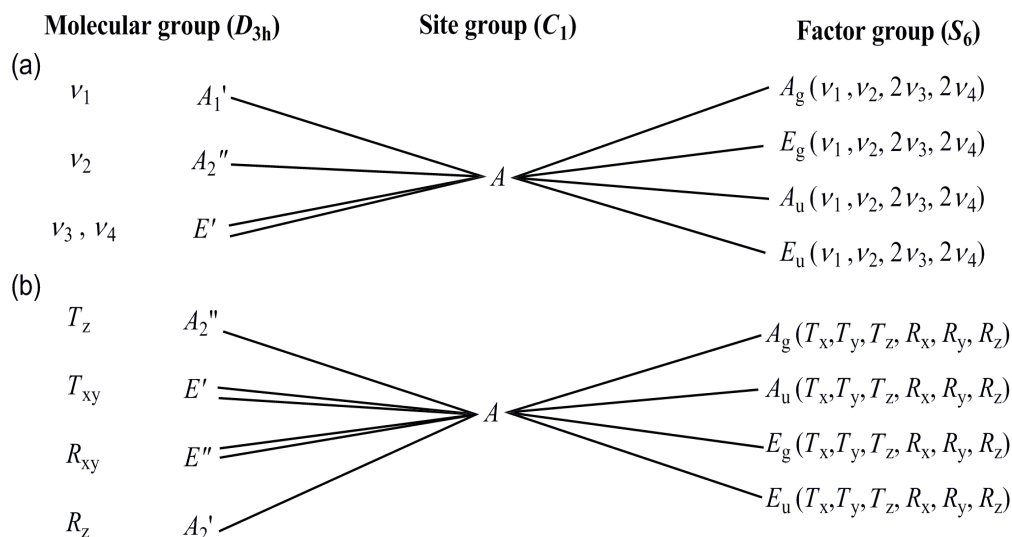


**Figure 10.** (a) Internal and (b) external  $\text{NO}_3^-$  modes in compound 2.

The isolated  $D_{3h}$  nitrate ion has three IR active ( $\nu_2$ – $\nu_4$ ) and three Raman active ( $\nu_1$ ,  $\nu_3$ , and  $\nu_4$ ) modes. In compound 2, ( $Z = 6$ ), the primitive cell contains 2 formula units ( $Z/3$ ), that is 6 nitrate anions, all being crystallographically equivalent. The site group is  $C_1$ , and the factor group is  $S_6$ . Accordingly, all bands become IR and Raman active (Figure 10). Six bands for both  $A_u$  and  $A_g$  symmetries and another six for both  $E_u$  and of  $E_g$  symmetries are expected, in the IR (the ungerade modes) and Raman (the gerade modes).

The components of the antisymmetric stretching modes of the nitrate ion in the IR spectrum of compound 2 are located at 1384 and 1309  $\text{cm}^{-1}$ , whereas the deuteration causes minor  $\sim 2 \text{ cm}^{-1}$  shifts of these positions, as is often the case because there are no pure group vibrations in reality (Figure 9b). In the Raman spectrum, only one very weak  $\nu_3(\text{NO}_3)$  Raman band was detected (Figure 9a). A possible coinciding band at 1288  $\text{cm}^{-1}$  in the IR appears at 1281  $\text{cm}^{-1}$  in the Raman spectrum and was assigned to the  $\nu(\text{CN})$  mode, whereas the  $\delta_s(\text{CH}_3)$  appears at 1427 both in the IR and Raman spectra. The strong singlet Raman band is also typical for  $\nu_s(\text{N-O})$  ( $\nu_1$ ) at 1044  $\text{cm}^{-1}$ , and the weak 719 and 713  $\text{cm}^{-1}$  Raman bands belong to  $\nu_4(\text{N-O})$ . A very weak Raman band was observed as  $\nu_2(\text{NO}_3)$  at 821  $\text{cm}^{-1}$ , and this mode was found also at 823  $\text{cm}^{-1}$  in the IR spectra of compound 2 and 2-**D**<sub>12</sub> as well (ESI Figures S14 and S16). In the IR spectrum, the band at 1044  $\text{cm}^{-1}$  hardly changes on deuteration, whereas the two neighboring bands are shifted by  $\sim 20 \text{ cm}^{-1}$ , which indicates that these bands belong to ligand groups, which are located close to N-H(N-D) groups, whereas the band to 1044  $\text{cm}^{-1}$  belongs to  $\nu_1(\text{N-O})$  band. This band shifts only to a minor extent (1  $\text{cm}^{-1}$ ) on deuteration which is comparable to the shift of other ( $\nu_3$ ) nitrate bands (Figure 9b,c). There are three translational ( $T_x$ ,  $T_y$ ,  $T_z$ ) and three rotational ( $R_x$ ,  $R_y$ ,  $R_z$ ) modes for  $A_u$ ,  $A_g$ ,  $E_u$ , and  $E_g$ , each, for the nitrate ions in compound 2, in the IR and Raman spectra (Figure 9a,b).

The correlation analysis of crystal water molecules is given in ESI Figure S17. For compound 2, the primitive cell contains 6 water molecules, all being crystallographically equivalent. Three normal modes ( $\nu_1$ ,  $\nu_2$ , and  $\nu_3$ ) are active in  $A_g$  and  $E_g$ , as well as in  $A_u$  and  $E_u$ , as Raman and IR active modes, respectively. Similarly, there are 6 external modes ( $T_x$ ,  $T_y$ ,  $T_z$ ,  $\rho$ ,  $\omega$ ,  $\tau$ ) both in  $A_g$  and  $E_g$  (Raman), and in  $A_u$  and  $E_u$  (IR) (ESI Figure S17).

The coordinated water in aqua complexes has several normal modes,  $\rho_r$ ,  $\rho_w$ ,  $\rho_t$ , and the  $\nu(\text{Fe-O})$  mode, the latter being one of the hindered translations. The  $\nu(\text{Fe-OH}_2)$  modes are found at  $436\text{ cm}^{-1}$  (the Fe-O modes from ligand carbonyl oxygen coordination are located in the far-IR region (Figure 11), at  $378/361\text{ cm}^{-1}$ ) [47,48]. These Fe-O modes were found in the Raman spectra at  $440\text{--}430$ ,  $417$ , and  $374\text{ cm}^{-1}$  (Figure 11). The deuteration of compound 2 induces a shift in the  $\nu(\text{Fe-O})$  band from  $436$  to  $427\text{ cm}^{-1}$ , thus this band belongs to a hindered translation Fe-OH<sub>2</sub> and the low wavenumber Fe-O band belongs to the  $\nu(\text{Fe-O})$  (*N,N*-dimethylurea-ligand) mode. The bands belonging to the normal modes ( $\rho_r$ ,  $\rho_w$ ,  $\rho_t$ ) of the coordinated and non-coordinated water can not be analyzed in detail, due to the complexity of this system). In what follows, we give a brief and tentative assignment. The non-coordinated H<sub>2</sub>O correlation analysis is given in ESI Figure S17. The  $\rho_w$  mode of water is assigned at  $547\text{ cm}^{-1}$  in the IR spectrum of compound 2. The lattice modes of compound 2 were found at  $320$ ,  $299$ ,  $250$ ,  $205$ , and  $147\text{ cm}^{-1}$  in the IR, whereas at  $311$ ,  $301$ ,  $280$ ,  $238$ ,  $208$ ,  $194$ , and  $107\text{ cm}^{-1}$  in the Raman spectrum.

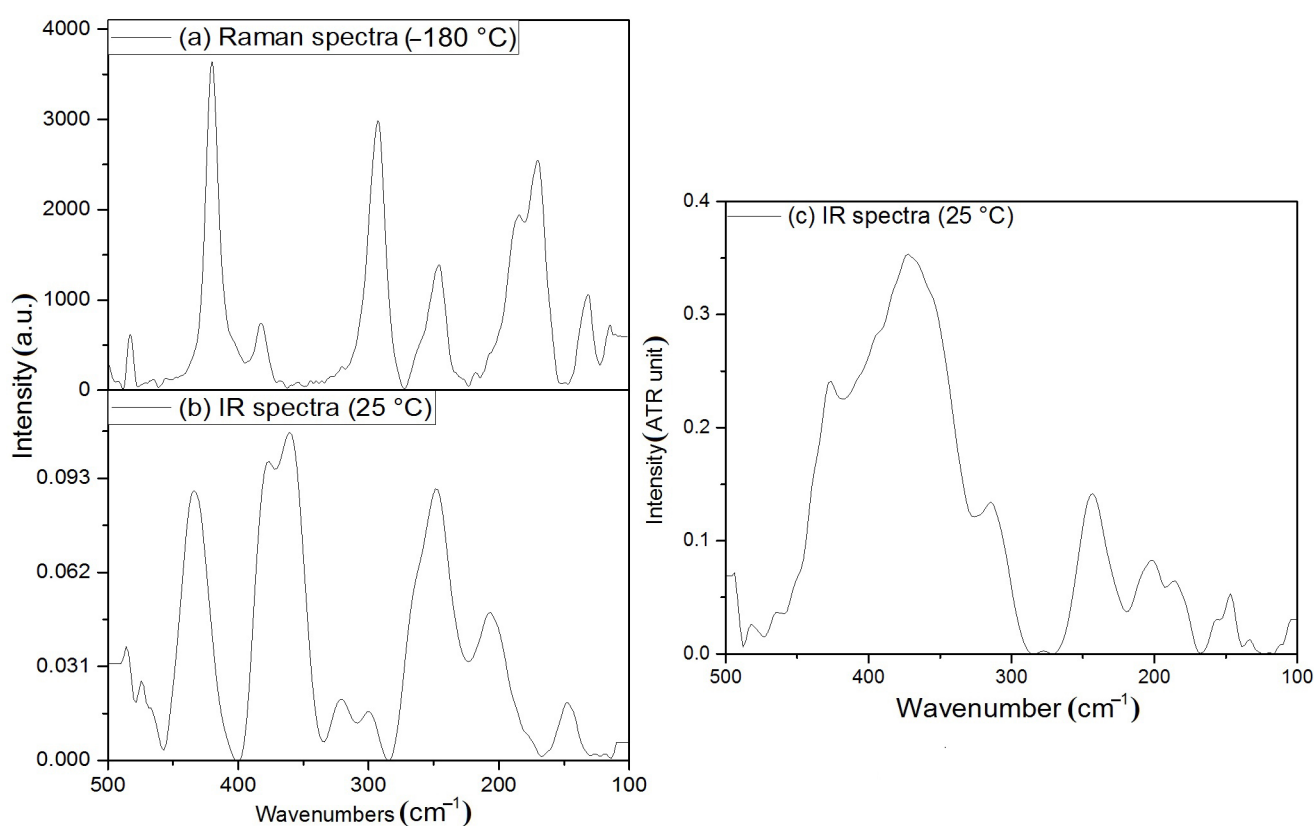


**Figure 11.** (a) Raman ( $-180\text{ }^{\circ}\text{C}$ ), (b) IR (room temperature) spectra of compound 2, and (c) IR (room temperature) spectra of compound 2-D<sub>12</sub> in the amide bands range.

### 3.4. UV Spectra of Compounds 1 and 2

Compounds 1 and 2 have only very weak absorption bands in their UV-Vis spectrum recorded in the solid phase (ESI Figure S18). Compounds 1 and 2 contain high-spin Fe<sup>III</sup> centers with  $6S$  ground terms, which do not split by crystal field. The electronic transitions in these complexes are both spin and Laporte forbidden, thus all the expected  $d-d$  bands are weak. From among the expected  $4T_{1g}(\text{G})\leftarrow 6S$ ,  $4T_{2g}(\text{G})\leftarrow 6S$ , and  $4A_g, 4E_g(\text{G})\leftarrow 6S$  transitions, the first one appears in the UV-Vis spectrum of compound 1 at  $757\text{ nm}$ , but this band was not observed in the spectrum of compound 2. The second type of transitions gives bands at  $540$  and  $490\text{ nm}$ , and the third ones appear at  $420$  and  $415\text{ nm}$ . The  $4A_g, 4E_g(\text{G})\leftarrow 6S$  transitions are degenerate in octahedral symmetry. The  $n-\pi^*$  and/or  $\pi-\pi^*$  bands of the nitrate and substituted urea ligands are located as a wide peak system in the UV spectra of compounds 1 and 2 centered around  $\sim 350\text{ nm}$  [2,49].

Numerous efforts have been made to measure the IR, Raman, and UV spectra of compound **3** as well; however, the crystals selected manually were deliquescent, and the compound decomposed during the sample preparations.

#### 4. Conclusions

Three octahedral iron(III) nitrate complexes with isomeric dimethylated urea ligands, namely [hexakis(*N,N'*-dimethylurea-O)iron(III)] nitrate (compound **1**), trans-[diaquatetrakis(*N,N*-dimethylurea-O)iron(III)] nitrate (compound **2**), and [hexakis(*N,N*-dimethylurea-O)iron(III)] nitrate trihydrate (compound **3**) were prepared. The single crystal structure and crystallographic parameters of complexes **1–3** were determined. The cation configurations including their intra and intermolecular hydrogen bonding systems were clarified.

In compound **1**, the complex cations are sandwiched between two nitrate anions and are arranged in columns running parallel to the crystallographic *c* direction. These nitrate ions have hydrogen bond interactions only with the complex cations in the neighboring columns and not with the cations that they straddle. Their interaction with the straddling nitrate ions is rather ionic. Between the nitrate-[Fe(*N,N'*-dimethylurea)<sub>6</sub>]<sup>3+</sup>-nitrate sandwiches, two strongly disordered nitrate anions fill the space each with half occupancy.

In compound **2**, layers of the complex cations are separated by nitrate layers. The [diaquatetrakis(*N,N*-dimethylurea-O)iron(III)]<sup>3+</sup> cations are able to form hydrogen bonds even axially, through their water ligands. The interconnecting NO<sub>3</sub><sup>−</sup> ions between the layers connect two types of complex cations *A* and *B* via hydrogen bonds. The three crystallographically different nitrate ions form four hydrogen bonds to one bidentate O atom and two monodentate O atoms. The spectroscopic characteristics of compound **2** were determined by low- and room temperature Raman, furthermore IR and far-IR measurements both on the non-deuterated and deuterated compound **2**.

In compound **3**, the complex cations form columns that are separated by distinct columns of the nitrate anions. The neighboring complex cations within one column do not have any hydrogen bond interactions with each other, they are only radially connected with the nitrate ions.

In compound **1**, the dimethylurea propellers screw in the opposite direction on the two sides of the complex, whereas in compound **3**, they are arranged with the same handedness on the two sides. The complexes have a helical chirality. The two sides of the complex cations differ in the hydrogen bond formation as well. On one side of the complex cation, the ligands form intermolecular hydrogen bonds only with the crystal waters; meanwhile, on the other side of the complex, the ligands form hydrogen bonds only with the nitrate ions.

**Supplementary Materials:** The following supporting information can be downloaded at: <https://www.mdpi.com/article/10.3390/cryst13071019/s1>, Figure S1: The calculated and the experimental powder X-ray diffraction of compound **1**; Figure S2: The calculated and the experimental powder X-ray diffraction of compound **2**; Figure S3: The low-temperature DSC of compound **1**; Figure S4: The low-temperature DSC of compound **2**; Figure S5: Coordination geometry of compound **3**; Figure S6: Intra- and intermolecular hydrogen bonding system in compound **3**; Figure S7: Intra- and intermolecular hydrogen bonding system in compound **2**; Figure S8: The Fe-Fe distances in compound **1**; Figure S9: The Fe-Fe distances in compound **3**; Figure S10: The Fe-Fe distances in compound **2**; Figure S11. (a) Far-range and (b) analytical range IR spectra of compound **1** at room temperature; Figure S12. Raman spectra of compound **1** at different temperatures; Figure S13: Raman and IR spectra of compound **1** in different wavenumber regions; Figure S14: (a) Close range and (b) Far-range IR spectra of compound **2**; (c) analytical and (d) Far-IR spectra of compound **2-D<sub>12</sub>**; Figure S15: Raman spectra of compound **2** at different temperatures; Figure S16: Raman and IR spectra of compound **2** and **2-D<sub>12</sub>** in 1100 and 700 cm<sup>−1</sup> wavenumber region; Figure S17. (a) Internal and (b) external H<sub>2</sub>O modes in compound **2**; Figure S18: UV-Vis spectra of compounds **1** and **2**; Table S1: Crystal data of urea/methylated urea compounds found in Cambridge Structural Database; Table S2: Bond lengths (Å) and angles (°) of compound **1**; Table S3: Torsion angles for compound **1** (°); Table S4: Bond lengths (Å) and angles (°) of compound **2**; Table S5: Torsion angles (°) of compound **2**; Table S6: Bond lengths (Å) and angles (°) of compound **3**; Table S7: Torsion angles (°) of compound **3**; Table S8: Analysis of

potential hydrogen bonds and schemes with  $d(D...A) < R(D) + R(A) + 0.50$ ,  $d(H...A) < R(H) + R(A) - 0.12$  Ang.,  $D-H...A > 100.0$  Deg in compound **1**; Table S9: Analysis of potential hydrogen bonds and schemes with  $d(D...A) < R(D) + R(A) + 0.50$ ,  $d(H...A) < R(H) + R(A) - 0.12$  [Å],  $D-H...A > 100.0$  ° in compound **2**; Table S10: Analysis of potential hydrogen bonds and schemes with  $d(D...A) < R(D) + R(A) + 0.50$ ,  $d(H...A) < R(H) + R(A) - 0.12$  (Å),  $D-H...A > 100.0$  ° in compound **3**; Table S11: Torsion angles (°) of nitrate ions in compound **2**; Table S12: Assignment of vibrational modes of compound **1**; Table S13: Assignment of vibrational modes of compound **2**.

**Author Contributions:** Conceptualization, L.K. and K.A.B.; formal analysis, V.M.P.; investigation, K.A.B., Z.H., L.B., Z.D. and A.F.; writing—original draft preparation, K.A.B. and L.K.; writing—review and editing, Z.H.; visualization, K.A.B. and L.B.; supervision, L.K. and Z.H. All authors have read and agreed to the published version of the manuscript.

**Funding:** The research was supported by the European Union and the State of Hungary, co-financed by the European Regional Development Fund (VEKOP-2.3.2-16-2017-00013) (L.K.) and the ÚNKP-21-3 and 22-3 New National Excellence Program of the Ministry for Innovation and Technology from the source of the National Research, Development, and Innovation Fund (K.A.B.). The crystallographic study was supported by the European Union and the State of Hungary and co-financed by the European Regional Development Fund (VEKOP-2.3.3-15-2017-00018).

**Data Availability Statement:** Not applicable.

**Acknowledgments:** We express our many thanks to Ildikó Filarszky for her help in the preparative work.

**Conflicts of Interest:** The authors declare no conflict of interest. The funders had no role in the design of the study; in the collection, analyses, or interpretation of data; in the writing of the manuscript; or in the decision to publish the results.

## References

1. Béres, K.A.; Homonnay, Z.; Kvitek, L.; Dürvanger, Z.; Kubikova, M.; Harmat, V.; Szilágyi, F.; Czégény, Z.; Németh, P.; Bereczki, L.; et al. Thermally Induced Solid-Phase Quasi-Intramolecular Redox Reactions of [Hexakis(urea-O)iron(III)] Permanganate: An Easy Reaction Route to Prepare Potential (Fe,Mn)O<sub>x</sub> Catalysts for CO<sub>2</sub> Hydrogenation. *Inorg. Chem.* **2022**, *61*, 14403. [[CrossRef](#)] [[PubMed](#)]
2. Béres, K.A.; Homonnay, Z.; Barta Holló, B.; Gracheva, M.; Petruševski, V.M.; Farkas, A.; Dürvanger, Z.s.; Kótai, L. Synthesis, structure, and Mössbauer spectroscopic studies on the heat-induced solid-phase redox reactions of hexakis(urea-O)iron(III) peroxodisulfate. *J. Mater. Res.* **2023**, *38*, 1102. [[CrossRef](#)]
3. Bereczki, L.; Petruševski, V.M.; Franguelli, F.P.; Béres, K.A.; Farkas, A.; Holló, B.B.; Czégény, Z.; Szilágyi, I.M.; Kótai, L. [Hexaamminecobalt(III)] Dichloride Permanganate—Structural Features and Heat-Induced Transformations into (Co<sup>II</sup>,Mn<sup>II</sup>)(Co<sup>III</sup>,Mn<sup>III</sup>)<sub>2</sub>O<sub>4</sub> Spinel. *Inorganics* **2022**, *10*, 252. [[CrossRef](#)]
4. Franguelli, F.P.; Kovács, É.; Czégény, Z.; Bereczki, L.; Petruševski, V.M.; Barta Holló, B.; Béres, K.A.; Farkas, A.; Szilágyi, I.M.; Kótai, L. Multi-Centered Solid-Phase Quasi-Intramolecular Redox Reactions of [(Chlorido)Pentaamminecobalt(III)] Permanganate—An Easy Route to Prepare Phase Pure CoMn<sub>2</sub>O<sub>4</sub> Spinel. *Inorganics* **2022**, *10*, 18. [[CrossRef](#)]
5. Müller, T.G.; Mogk, J.; Conrad, M.; Kraus, F. Octaammine Eu<sup>II</sup> and Yb<sup>II</sup> Azides and Their Thermal Decompositions to the Nitrides. *Eur. J. Inorg. Chem.* **2016**, *26*, 4162–4169. [[CrossRef](#)]
6. Hetmanczyk, L.; Hetmanczyk, J. Comparison of vibrational dynamics, thermal behaviour, and phase transition in [Ni(NH<sub>3</sub>)<sub>4</sub>](ReO<sub>4</sub>)<sub>2</sub> and [Ni(NH<sub>3</sub>)<sub>6</sub>](ReO<sub>4</sub>)<sub>2</sub>. *J. Therm. Anal. Calorim.* **2015**, *119*, 1415–1428. [[CrossRef](#)]
7. Fogaca, L.A.; Kovács, É.; Németh, G.; Kamarás, K.; Béres, K.A.; Németh, P.; Petruševski, V.; Bereczki, L.; Holló, B.B.; Sajó, I.E.; et al. Solid-Phase Quasi-Intramolecular Redox Reaction of [Ag(NH<sub>3</sub>)<sub>2</sub>]<sub>2</sub>MnO<sub>4</sub>: An Easy Way to Prepare Pure AgMnO<sub>2</sub>. *Inorg. Chem.* **2021**, *60*, 3749. [[CrossRef](#)] [[PubMed](#)]
8. Fogaça, L.A.; Bereczki, L.; Petruševski, V.M.; Barta-Holló, B.; Franguelli, F.P.; Mohai, M.; Béres, K.A.; Sajó, I.E.; Szilágyi, I.M.; Kótai, L. A Quasi-Intramolecular Solid-Phase Redox Reaction of Ammonia Ligands and Perchlorate Anion in Diamminesilver(I) Perchlorate. *Inorganics* **2021**, *9*, 38. [[CrossRef](#)]
9. Kovács, G.B.; May, N.v.; Bombicz, P.A.; Klébert, S.; Németh, P.; Menyhárd, A.; Novodárszki, G.; Petruševski, V.; Franguelli, F.P.; Magyari, J.; et al. An Unknown Component of a Selective and Mild Oxidant: Structure and Oxidative Ability of a Double Salt-Type Complex Having κ<sup>1</sup> O-Coordinated Permanganate Anions and Three- and Four-Fold Coordinated Silver Cations. *RSC Adv.* **2019**, *9*, 28387. [[CrossRef](#)]
10. Solt, H.E.; Németh, P.; Mohai, M.; Sajó, I.E.; Klébert, S.; Franguelli, F.P.; Fogaca, L.A.; Pawar, R.P.; Kótai, L. Temperature-Limited Synthesis of Copper Manganites along the Borderline of the Amorphous/Crystalline State and Their Catalytic Activity in CO Oxidation. *ACS Omega* **2021**, *6*, 1523. [[CrossRef](#)]

11. Franguelli, F.P.; Barta-Holló, B.; Petruševski, V.M.; Sajó, I.E.; Klébert, S.; Farkas, A.; Bódis, E.; Szilágyi, I.M.; Pawar, R.P.; Kótai, L. Thermal Decomposition and Spectral Characterization of Di[Carbonatotetraamminecobalt(III)] Sulfate Trihydrate and the Nature of Its Thermal Decomposition Products. *J. Therm. Anal. Calorim.* **2021**, *145*, 2907. [[CrossRef](#)]
12. Trif, L.; Franguelli, F.P.; Lendvay, G.; Majzik, E.; Béres, K.; Bereczki, L.; Szilágyi, I.M.; Pawar, R.P.; Kótai, L. Thermal Analysis of Solvatomorphic Decakis (Dimethylammonium) Dihydrogendodecatungstate Hydrates. *J. Therm. Anal. Calorim.* **2021**, *144*, 81. [[CrossRef](#)]
13. Petrushevski, V.M.; Béres, K.A.; Bombicz, P.; Farkas, A.; Kótai, L.; Bereczki, L. Structural and Raman Spectroscopic Characterization of Tetrpyridinesilver(I) Perrhenate, [Agpy<sub>4</sub>]ReO<sub>4</sub>. *Maced. J. Chem. Chem. Eng.* **2022**, *41*, 37. [[CrossRef](#)]
14. May, N.V.; Bayat, N.; Béres, K.A.; Bombicz, P.; Petruševski, V.M.; Lendvay, G.; Farkas, A.; Kótai, L. Structure and Vibrational Spectra of Pyridine Solvated Solid Bis(Pyridine)Silver(I) Perchlorate, [Agpy<sub>2</sub>ClO<sub>4</sub>].0.5py. *Inorganics* **2022**, *10*, 123. [[CrossRef](#)]
15. Mehrotra, R.N. Review on the chemistry of [M(NH<sub>3</sub>)<sub>n</sub>](XO<sub>4</sub>)<sub>m</sub> (M=transition metal, X=Mn, Tc or Re, n=1–6, m=1–3) ammine complexes. *Inorganics*, 2023; 2023050956, *accepted for publication*.
16. Hu, B.; Frueh, S.; Garces, H.F.; Zhang, L.; Aindow, M.; Brooks, C.; Kreidler, E.; Suib, S.L. Selective Hydrogenation of CO<sub>2</sub> and CO to Useful Light Olefins over Octahedral Molecular Sieve Manganese Oxide Supported Iron Catalysts. *Appl. Catal. B* **2013**, *132*, 54. [[CrossRef](#)]
17. Jiang, J.; Wen, C.; Tian, Z.; Wang, Y.; Zhai, Y.; Chen, L.; Li, Y.; Liu, Q.; Wang, C.; Ma, L. Manganese-Promoted Fe<sub>3</sub>O<sub>4</sub> Microsphere for Efficient Conversion of CO<sub>2</sub> to Light Olefins. *Ind. Eng. Chem. Res.* **2020**, *59*, 2155. [[CrossRef](#)]
18. Liu, B.; Geng, S.; Zheng, J.; Jia, X.; Jiang, F.; Liu, X. Unravelling the New Roles of Na and Mn Promoter in CO<sub>2</sub> Hydrogenation over Fe<sub>3</sub>O<sub>4</sub>-Based Catalysts for Enhanced Selectivity to Light  $\alpha$ -Olefins. *ChemCatChem* **2018**, *10*, 4718. [[CrossRef](#)]
19. Liu, Y.; Chen, J.-F.; Bao, J.; Zhang, Y. Manganese-Modified Fe<sub>3</sub>O<sub>4</sub> Microsphere Catalyst with Effective Active Phase of Forming Light Olefins from Syngas. *ACS Catal.* **2015**, *5*, 3905. [[CrossRef](#)]
20. Okaya, Y.; Pepinsky, R.; Takeuchi, Y.; Kuroya, H.; Shimida, A.; Gallitelli, P.; Stemple, N.; Beevers, A. X-ray analyses of some complex-ion structures. *Acta Crystallogr.* **1957**, *10*, 798.
21. Kuz'mina, N.E.; Palkina, K.K.; Savinkina, E.V.; Kozlova, I.A. Products of Reactions of Manganese(II) and Iron(II) Iodides with Urea: Comparison of Structures and Properties. *Zh. Neorg. Khim.* **2000**, *45*, 332–337.
22. Galeazzi, G.; Russo, U.; Valle, G.; Calogero, S. Mössbauer study of some iron(III) complexes with urea type ligands and the crystal structure of hexakisdimethylureairon(III) perchlorate. *Transit. Met. Chem.* **1981**, *6*, 325. [[CrossRef](#)]
23. Russo, U.; Calogero, S.; Pra, A.D. Characterization of some high-spin iron(III) complexes with urea derivatives. Crystal structure of diaquatetrakis(perhydropyrimidin-2-one)iron trichloride dihydrate and of perhydropyrimidin-2-one. *J. Chem. Soc. Dalton Trans.* **1980**, *4*, 646.
24. Carp, O.; Patron, L.; Diamandescu, L.; Reller, A. Thermal decomposition study of the coordination compound [Fe(urea)<sub>6</sub>](NO<sub>3</sub>)<sub>3</sub>. *Thermochim. Acta* **2002**, *390*, 169. [[CrossRef](#)]
25. Zhao, S.; Sin, A. Synthesis of iron(III)-urea complex in organic solvent and its thermal decomposition. *Huaxue Shiji* **2010**, *32*, 108.
26. Theophanides, T.; Harvey, P.D. Structural and spectroscopic properties of metal-urea complexes. *Coord. Chem. Rev.* **1987**, *76*, 237. [[CrossRef](#)]
27. Drakopoulou, L.; Papatrifiantafyllopoulou, C.; Terzis, A.; Perlepes, S.P.; Manessi-Zoupa, E.; Papaefstathiou, G.S. Synthesis, X-Ray Structure, and Characterization of a Complex Containing the Hexakis(urea)cobalt(II) Cation and Lattice Urea Molecule. *Bioinorg. Chem. Appl.* **2007**, *2007*, 51567. [[CrossRef](#)]
28. Bala, R.; Sachdeva, D.; Kumar, M.; Parakash, V. Advances in coordination chemistry of hexaurea complexes of chromium(III). *J. Coord. Chem.* **2020**, *73*, 2801. [[CrossRef](#)]
29. Aghabozorg, H.; Palenik, G.J.; Stoufer, R.C.; Summers, J. Dynamic Jahn-Teller effect in a manganese(III) complex. Synthesis and structure of hexakis(urea)manganese(III) perchlorate. *Inorg. Chem.* **1982**, *21*, 3903. [[CrossRef](#)]
30. Figgis, B.N.; Wadley, L.G.B.; Graham, J. Crystal structure of hexaurea salts of trivalent metals. I. Ti(urea)<sub>6</sub>(ClO<sub>4</sub>)<sub>3</sub> at room temperature. *Acta Cryst.* **1972**, *28*, 187. [[CrossRef](#)]
31. Russo, U.; Calogero, S.; Burriesci, N.; Petrera, M. Mössbauer characterization of some new high-spin iron complexes with urea and thiourea derivatives. *J. Inorg. Nucl. Chem.* **1979**, *41*, 25. [[CrossRef](#)]
32. Yamauchi, S.; Sakai, Y.; Tominaga, T. Paramagnetic relaxation effects on Mössbauer spectra of hexakis/alkylurea/iron(III)/complexes. *J. Radioanal. Nucl. Chem.* **1987**, *119*, 283. [[CrossRef](#)]
33. Yamauchi, S.; Sakai, Y.; Nishioji, H.; Tominaga, T. Mössbauer spectroscopic study of the magnetic relaxation in tris( $\beta$ -diketonato)iron(III) complexes. *Int. J. Appl. Radiat. Isot.* **1983**, *34*, 977. [[CrossRef](#)]
34. Martiz, A.; Károly, Z.; Domján, A.; Mohai, M.; Bereczki, L.; Trif, L.; Farkas, A.; László, K.; Menyhárd, A.; Kótai, L. Nano-ZrO<sub>2</sub>@C, Nano-(ZrC, ZrO<sub>2</sub>)@C and Nano-ZrC@C Composites Prepared by Plasma-Assisted Carbonization of Zr-Loaded Iminodiacetate-Functionalized Styrene-Divinylbenzene Copolymers. *Inorganics* **2022**, *10*, 77. [[CrossRef](#)]
35. Martiz, A.; Károly, Z.; Trif, L.; Mohai, M.; Bereczki, L.; Németh, P.; Molnár, Z.; Menyhárd, A.; Pawar, R.P.; Tekale, S.; et al. Plasma-assisted preparation of nano-(ZrC, ZrO<sub>2</sub>)@ carbon composites from Zr-loaded sulfonated styrene-divinylbenzene copolymers. *J. Therm. Anal. Calorim.* **2022**, *147*, 9353–9365. [[CrossRef](#)]
36. Sheldrick, G.M. SHELXT—Integrated space-group and crystal-structure determination. *Acta Crystallogr. A* **2015**, *71*, 3. [[CrossRef](#)]
37. Sheldrick, G.M. Crystal structure refinement with SHELXL. *Acta Crystallogr. C Struct. Chem.* **2015**, *71*, 3. [[CrossRef](#)]

38. Dolomanov, O.V.; Bourhis, L.J.; Gildea, R.J.; Howard, J.A.K.; Puschmann, H. OLEX2: A complete structure solution, refinement and analysis program. *J. Appl. Crystallogr.* **2009**, *42*, 339. [[CrossRef](#)]
39. Macrae, C.F.; Sovago, I.; Cottrell, S.J.; Galek, P.T.A.; McCabe, P.; Pidcock, E.; Platings, M.; Shields, G.P.; Stevens, J.S.; Towler, M.; et al. Mercury 4.0: From visualization to analysis, design and prediction. *J. Appl. Crystallogr.* **2020**, *53*, 226. [[CrossRef](#)]
40. Kocsis, T.; Magyari, J.; Sajó, I.E.; Pasinszki, T.; Homonnay, Z.; Szilágyi, I.M.; Farkas, A.; May, Z.; Effenberger, H.; Szakáll, S.; et al. Evidence of quasi-intramolecular redox reactions during thermal decomposition of ammonium hydroxodisulfiteferriate(III),  $(\text{NH}_4)_2[\text{Fe}(\text{OH})(\text{SO}_3)_2] \cdot \text{H}_2\text{O}$ . *J. Therm. Anal. Calorim.* **2018**, *132*, 493. [[CrossRef](#)]
41. Smeets, S.; Lutz, M. Hexakis(urea- $\kappa\text{O}$ )zinc(II) dinitrate at 110 and 250 K: Uniaxial negative thermal expansion. *Acta Crystallogr. C Struct. Chem.* **2011**, *67*, 50. [[CrossRef](#)] [[PubMed](#)]
42. Kuz'mina, N.E.; Palkina, K.K.; Savinkina, E.V.; Kuznetsova, N.T.; Kozlova, I.A. Syntheses and Crystal Structures of Nickel(II) and Cobalt(II) Urea Diiododates  $[\text{Ni}(\text{CON}_2\text{H}_4)_6][\text{I}_3]_2 \cdot 2(\text{CON}_2\text{H}_4)$  and  $[\text{Co}(\text{CON}_2\text{H}_4)_6][\text{I}_3]_2 \cdot 2(\text{CON}_2\text{H}_4)$ . *Zh. Neorg. Khim.* **2000**, *45*, 780.
43. Palkina, K.K.; Kuz'mina, N.E.; Orlova, V.; Kondokova, I. Coordination Compounds of Some Transition Metal, Magnesium, and Calcium Nitrates with Dimethylurea. *Zh. Neorg. Khim.* **1999**, *44*, 963.
44. Figgis, B.N.; Skelton, B.W.; White, A.H. Crystal structures of hexa(N-methylurea)cobalt(II) sulfate and thiosulfate. *Aust. J. Chem.* **1980**, *33*, 425. [[CrossRef](#)]
45. Masłowska, J.; Cedzyńska, K. The structure of iron(III) complexes with carbamide derivatives. *J. Mol. Struct.* **1973**, *19*, 521. [[CrossRef](#)]
46. Mido, Y.; Murata, H. Infrared Absorption Spectra of Urea-formaldehyde Initial Condensation Products. II. Dimethylurea. *Bull. Chem. Soc. JPN* **1969**, *42*, 3372. [[CrossRef](#)]
47. Penland, R.B.; Lane, T.J.; Quagliano, J.V. Infrared Absorption Spectra of Inorganic Coordination Complexes. VII. Structural Isomerism of Nitro- and Nitritopentamminecobalt(III) Chlorides. *J. Am. Chem. Soc.* **1956**, *78*, 887. [[CrossRef](#)]
48. Cotton, S.A.; Gibson, J.F. Electron paramagnetic resonance and vibrational spectra of some iron(III) complexes with oxygen-containing ligands. *J. Chem. Soc. A* **1971**, 1690. [[CrossRef](#)]
49. Butorc, V.; Simeon, V.; Tomisic, V. Effect of temperature on the UV spectra of concentrated  $\text{NaNO}_3$  aqueous solutions. *Croat. Chem. Acta* **2007**, *80*, 533.

**Disclaimer/Publisher's Note:** The statements, opinions and data contained in all publications are solely those of the individual author(s) and contributor(s) and not of MDPI and/or the editor(s). MDPI and/or the editor(s) disclaim responsibility for any injury to people or property resulting from any ideas, methods, instructions or products referred to in the content.